A Mathematical Study of Volume Shifts and Ionic Concentration Changes during Ischemia and Hypoxia.

Chung-Seon Yi, Aaron L. Fogelson, James P. Keener

Department of Mathematics

University of Utah

Salt Lake City, Utah 84112

Charles S. Peskin

Courant Institute of Mathematical Sciences

and Center for Neural Science

New York University

251 Mercer Street

New York, NY 10012

August 9, 2002

Submitted to Journal of Theoretical Biology – REVISED

Address for correspondence:

Aaron Fogelson

Department of Mathematics

155 South 1400 East, 233 JWB

University of Utah

Salt Lake City, UT 84112

fogelson@math.utah.edu

Phone: (801) 581-8150

Fax: (801) 585-1640

Abstract The response of tissue to ischemia (cessation of blood flow and deprivation of oxygen) includes swelling of the intracellular space, shrinkage of the extracellular space, and an increase in the extracellular potassium concentration. The responses of cardiac and brain tissue to ischemia are qualitatively different in that cardiac tissue shows a rise in extracellular potassium over several minutes from about 5 to 10-12 mM followed by a plateau, while brain tissue shows a similar initial rise followed by a very rapid increase in extracellular potassium to levels of 50-80 mM. During hypoxia the flow of blood (or perfusate) is maintained and, while there is a substantial efflux of potassium from cells, there is little accumulation of potassium in the interstitium. A mathematical model is proposed and studied to try to elucidate the mechanism(s) underlying the increase in extracellular potassium, and the different timecourses seen in neural and cardiac tissue. The model involves a Hodgkin-Huxley type description of transmembrane ion currents, allows for ion concentrations as well as volumes to change for both the intracellular and extracellular space, and includes coupling of damaged tissue to nearby healthy tissue. The model produces a response to ischemia much like that seen in neural tissue, and the mechanism underlying this response in the model is determined. The same mechanism is not present in cardiac ion models, and this may explain the qualitative difference in response shown in cardiac tissue.

INTRODUCTION

Ischemia is a situation in which blood flow and oxygen transport to a tissue has stopped. It is well known that in many tissues extracellular potassium increases significantly in response to ischemia, and this increase may have important pathological consequences. In particular, in cardiac ischemia, the increased extracellular potassium concentration may contribute to the onset of arrhythmias. While many hypotheses have been offered for the mechanism of extracellular potassium increase, no model based on these hypotheses has succeeded in accounting for a rapid and substantial rise in the extracellular potassium concentration. The goal of this paper is to examine the extent to which the rise of extracellular potassium can be explained by a simple ionic model in which intra- and extracellular ion concentrations and intra- and extracellular volumes are allowed to vary.

The experimental data on extracellular potassium rise, which we review below, is quite varied. In particular the timecourse and magnitude of the rise differed from one experiment to the next either because the tissues examined or the experimental protocols were different. The experimental data for any one tissue, e.g., ventricular myocardial or neural tissue, are not clear nor complete enough to warrant an attempt at a quantitative match with the experiments. Instead we explore the qualitative behavior of the model and show that it can capture some of the important features of the experimental results.

While ischemia refers to the cessation of both blood flow and oxygen transport to a tissue, hypoxia refers to a condition of normal perfusion but reduction of the supply of oxygen below that needed to meet the oxygen requirements of the tissue. For both hypoxia and ischemia, depriving the tissue of oxygen causes cells in the tissue to switch from aerobic glucose processing to anerobic processing with a consequent large reduction in ATP production. The diminished supply of ATP reduces the effectiveness of the cell membrane ion pumps, particularly the Na-K-ATPase pump, and limits the cell's ability to maintain homeostasis. In the case of ischemia, the cessation of blood flow has additional effects including a reduced supply of metabolic substrates, reduced removal of waste products (among which are lactate, H^+, and inorganic phosphate), and accumulation of potassium in the extracellular space.

Ischemia and hypoxia have been studied in a wide variety of animals, tissues, and preparations. Hansen (1978) studied ischemia in the brain tissue of living rats that were put into cardiac arrest; Hrabetova et al. (2002) studied ischemia in isolated 1 mm thick slices of brain tissue bathed in artificial cerebrospinal fluid; Yan et al. (1993) and Yan et al. (1996) examined ischemia and hypoxia in isolated blood-perfused rabbit papillary muscles; Hill and Gettes (1980) studied regional ischemia induced in pig hearts by ligature of the left anterior coronary artery; and Fiolet et al. (1993) investigated ischemia in suspensions of isolated rat ventricular myocytes, and in whole heart preparations.

For ischemic neural tissue, Hansen (1978) reported a biphasic increase in $[K^+]_e$, with a very rapid rise to 50–60 mM followed by a slower rise to 80 mM as shown in Figure (1a). Hrabetova et al. (2002) similarly reported an initial rise of $[K^+]_e$ in brain tissue slices to 50 mM. During myocardial ischemia, the myocytes swell, the extracellular space shrinks by about 20% in 20 minutes (Yan et al. 1996; Fiolet et al. 1993), and there is a three-phase change in the extracellular potassium concentration $[\mathrm{K}^+]_e$. The three phases are generally described as consisting of a rapid increase, relative plateau, and second slower increase as shown in Figure (1b). It should be emphasized that although the word 'rapid' is used in both the neural and cardiac contexts, the rise in extracellular potassium in the cardiac case occurs much more slowly and to a much lower level than for the neural tissue; the behavior of the extracellular potassium concentration is qualitatively different in brain ischemia and cardiac ischemia. For cardiac tissue, the duration of the first rapid rise phase, the height of the plateau, and the steepness of the second rise varied with species, experimental protocol (e.g., whether the myocytes were quiescent or stimulated electrically), and location of the measurement relative to the distance to nonischemic tissue (Hill and Gettes 1980; Wilde et al. 1990). During the initial rapid rise phase $[K^+]_e$ increased from its normal levels of 4-5 mM to 11-20 mM. The plateau phase began 5 to 15 minutes after the onset of ischemia, and the third, slow rise, phase began 15 to 30 minutes after the onset. In contrast, during normal flow hypoxia in cardiac myocytes, $[K^+]_e$ rose very little, although the efflux of potassium from the cells to the extracellular space was more than 8 times that during ischemia (Yan et al. 1993).

Data for the timecourse of intracellular ATP levels during ischemia are sparse. Jennings and Reimer (1991) reported ATP levels in an open chest anesthetized dog heart as 67%, 35%, and less than 10% of normal after 5, 15, and 40 minutes of ischemia, while Fiolet et al. (1993) reported ATP levels of 93%, 67% and 11% of normal after 7.5, 15, and 30 minutes of ischemia in myocyte suspensions. The lack of data is compounded by uncertainty about what ATP was actually measured in light of new information that within cells ATP is subdivided into separate pools based on where it is produced and used (Weiss and Korge 2001). Thus, the cited ATP levels may have little to do with the ATP levels in the neighborhood of cell plasma membrane and its Na-K-ATPase pumps. The correlation between measured [ATP] and Na-K-ATPase activity is further weakened by the effect of intracellular pH on pump activity. As the cells switch to anaerobic ATP production, lactic acid is produced. This reduces the intracellular pH and slows the Na-K-ATPase pump. In the model that follows we use Jennings and Reimer (1991)'s ATP data to give a rough idea of the timecourse of the decline in Na-K-ATPase activity. A good fit to Jenning's data is given by $[\mathrm{ATP}](t) = [\mathrm{ATP}]_{\max} \cdot (0.35)^{(t/15)}$, where t is measured in minutes (see Figure 2).

The purpose of this paper is to explore mechanisms for extracellular potassium accumulation during ischemia, and to capture and understand the different responses to ischemia and hypoxia. Existing detailed models of cardiac ionic behavior such as the Ruo-Ludy model II (Luo and Rudy 1991) and the Noble model (1991) (Noble et al. 1991) of single cells do not consider extracellular volume as a variable, and do not consider the effect of capillary flow or its cessation on ion concentrations, or the effects of nearby healthy tissue. The model proposed here includes these effects, using a simpler Hodgkin-Huxley type ionic model for this initial study. The model describes events in a tissue consisting of a *collection* of homogeneous cells subject to ischemia or hypoxia, a homogeneous extracellular space surrounding these cells, a capillary compartment representing the vasculature for this piece of tissue, and another compartment corresponding to the healthy tissue surrounding the ischemic or hypoxic tissue. The first three compartments are collectively referred to as the 'damaged' tissue. Below we give a detailed derivation and discussion of equations describing ion concentrations, volumes, and voltages in these four regions. Two

unusual components of the modeling are the difficulty in building a model whose steady states are stable over the long-term, and the need to couple the damaged region to a surrounding healthy region in order to get reasonable reductions in extracellular volume and increases in extracellular potassium concentration.

MATHEMATICAL MODEL

We consider four compartments as displayed in Figure 3. In the tissue damaged by ischemia or hypoxia we assume there are three well-mixed compartments representing the intracellular space within a collection of homogeneous cells, the extracellular space surrounding these cells, and the capillary space serving the cells. In addition, we include a fourth compartment representing the extracellular space of the surrounding undamaged tissue. This compartment is also assumed to be spatially homogeneous. The cell membrane separates the intracellular space from the extracellular space, and the capillary wall separates the extracellular space from the capillary space. The volumes of the intracellular and extracellular spaces are allowed to vary. We assume that there are three solutes, sodium (Na^+), potassium (K^+), chloride (Cl^-) to which the cell membrane and capillary wall are permeable. We also assume that each compartment contains charged protein molecules (or other charged macromolecules) which cannot move between compartments. Ions move between the extracellular space and the capillary because of electrochemical potential gradients, and between the extra- and intra-cellular space because of potential gradients and pumps.

All spaces are assumed to be electrically neutral, and the three spaces within the damaged region are assumed to have the same hydrostatic pressure. Water and ions can be exchanged between the damaged intracellular and extracellular space and the capillary, and between the damaged extracellular space and the surrounding normal tissue. The fluxes of ions and water are determined by electrochemical potential gradients, osmotic pressure differences, and in the case of fluxes between the damaged and healthy extracellular spaces, by the hydrostatic pressure difference induced by volume changes in the damaged region. We also assume that the capillary wall is highly permeable to water and ions.

We next present equations which model the electro-chemical balance and volume regulation for the situation just described. We denote ion concentrations by $[\mathrm{Na}^+]$, $[\mathrm{K}^+]$ and $[\mathrm{Cl}^-]$ with subscripts 'i' for the intracellular space, 'e' for the extracellular space, 'a' for arterial blood, and 'v' for venous blood. V_i and V_e denote the volume of the intra- and extracellular space respectively, δ_i and δ_e denote voltage in these spaces, with the voltage in the capillary space used

as the reference voltage, and taken to be zero.

The dynamics of the intracellular quantities are described by the equations:

$$\frac{d(V_i[Na^+]_i)}{dt} = -\left\{\frac{g_{\mathrm{Na}}}{F}\left(\delta_i - \delta_e - \delta_{Na}\right) + 3\cdot P\right\}, \quad (1)$$

$$\frac{d(V_i[K^+]_i)}{dt} = -\left\{\frac{g_{\mathrm{K}}}{F}\left(\delta_i - \delta_e - \delta_{K}\right) - 2\cdot P\right\}, \quad (2)$$

$$\frac{d(V_i[Cl^-]_i)}{dt} = \left\{\frac{g_{\mathrm{Cl}}}{F}\left(\delta_i - \delta_e + \delta_{Cl}\right)\right\}, \quad (3)$$

$$0 = [Na^+]_i + [K^+]_i - [Cl^-]_i - \frac{z_i X_i}{V_i}, \quad (4)$$

$$\frac{dV_i}{dt} = L_p^{ie}\cdot(\Pi_i - \Pi_e). \quad (5)$$

$$(6)$$

Equations (1)–(3) express the fact that the number of each type of ion in the intracellular space changes only because of fluxes of those ions across the cell membrane. These fluxes are assumed to be described by a Hodgkin-Huxley type current. For an ion S with valence z, the Nernst potential is defined as

$$\delta_{\mathrm{S}} = \frac{RT}{zF}\ln\left(\frac{[\mathrm{S}]_e}{[\mathrm{S}]_i}\right),$$

where R is the universal gas constant , T is the absolute temperature, and F is Faraday's constant. When the transmembrane potential $\delta_i - \delta_e$ is equal to an ion's Nernst potential, there is no net flux of that ion. It is important to note that the Nernst potentials in our model are dynamic, changing as the intracellular and extracellular ionic concentrations change. Equations (1) and (2) also include the flux due to the Na-K ATP-driven pump which exchanges three sodium ions for two potassium ions. In general, the pump rate P depends on transmembrane voltage and ion concentrations. Note that positive flux terms (the expressions in $\{\}$) correspond to outward movement of ions. In Equations (1)–(3), g_{Na}, g_{K} and g_{Cl} denote membrane conductances.

Equation (4) expresses our assumption that the intracellular region is electrically neutral. This is a good approximation to the real situation in which excess charge can accumulate only in a thin region near the cell membrane. The excess charge equation is

$$RT\left([Na^+]_i + [K^+]_i - [Cl^-]_i - \frac{z_i\cdot X_i}{V_i}\right) = \frac{C_m A_S}{V_i F}\left(\delta_i - \delta_e\right).$$

Here C_m is the capacitance (per unit area) of the cell membrane. X_i is the number of protein molecules in the intracellular space, z_i is the average number of charges on each protein molecule, and A_S is the surface area of the cell. The nondimensional capacitance $(A_S\, C_m\, RT)/(F^2\, V_i\, [K^+]_i{}^*) \approx 10^{-6}$ is small enough to be ignored, and Equation (4) results. Here, $[K^+]_i{}^*$ is the normal intracellular potassium concentration.

Equation (5) describes how intracellular volume changes in response to an osmotically-driven flow of water across the cell membrane. This equation expresses Starling's law of membrane filtration (Fung 1990): For two dilute solutions separated by a semipermeable membrane, the flow across the membrane is proportional to the driving force $(\Delta P - \Delta\Pi)$, where ΔP and $\Delta\Pi$ are, respectively, the hydrostatic and osmotic pressure differences across the membrane. Animal cell membranes cannot withstand a nonzero hydrostatic pressure difference, so we set $\Delta P = 0$. The osmotic pressure is given by $\Pi = RTC$ where C is the total concentration of solute particles in the fluid. Note that this relation is the same as the ideal gas law. The osmotic pressure in the intracellular space is defined by the expression

$$\Pi_i = RT \cdot \left([Na^+]_i \; + \; [K^+]_i \; + \; [Cl^-]_i \; + \; \frac{X_i}{V_i} \right)$$

while the osmotic pressure in the extracellular space is given by

$$\Pi_e = RT \cdot \left([Na^+]_e \; + \; [K^+]_e \; + \; [Cl^-]_e \; + \; \frac{X_e}{V_e} \right)$$

In equation (5) the flux of water across the membrane is the osmotic pressure difference multiplied by a permeability coefficient L_p^{ie}.

The equations for the extracellular quantities are similar to those for the intracellular com-

partment:

$$\frac{d(V_e[Na^+]_e)}{dt} = \left\{\frac{g_{\mathrm{Na}}}{F}(\delta_i - \delta_e - \delta_{Na}) + 3\cdot P\right\} - J^v_{\mathrm{Na}} - J^h_{\mathrm{Na}}, \quad (7)$$

$$\frac{d(V_e[K^+]_e)}{dt} = \left\{\frac{g_{\mathrm{K}}}{F}(\delta_i - \delta_e - \delta_K) - 2\cdot P\right\} - J^v_{\mathrm{K}} - J^h_{\mathrm{K}}, \quad (8)$$

$$\frac{d(V_e[Cl^-]_e)}{dt} = -\left\{\frac{g_{\mathrm{Cl}}}{F}(\delta_i - \delta_e + \delta_{Cl})\right\} - J^v_{\mathrm{Cl}} - J^h_{\mathrm{Cl}}, \quad (9)$$

$$0 = [Na^+]_e + [K^+]_e - [Cl^-]_e - \frac{z_e X_e}{V_e}, \quad (10)$$

$$\frac{dV_e}{dt} = L^{ie}_p \cdot (\Pi_e - \Pi_i) - J^v_{\mathrm{H_2O}} - J^h_{\mathrm{H_2O}}. \quad (11)$$

There are ordinary differential equations for the number of each ion in the space (Na^+, K^+, Cl^- equations (7) - (9)), an equation (10) expressing electroneutrality, and an equation (11) governing extracellular volume. Equations (7), (8), (9) and (11) include exactly the same fluxes as those in the intracellular equations (1), (2), (3) and (5), respectively but with opposite signs. However, while the cell only communicates with the interstitium, the extracellular space communicates with the cell, the capillary and the nearby normal (healthy) tissue. Therefore, it is necessary to have additional flux terms, J^v_{Na}, J^v_{K}, J^v_{Cl}, $J^v_{\mathrm{H_2O}}$ for fluxes from the extracellular space to the capillary (vascular space), and J^h_{Na}, J^h_{K}, J^h_{Cl}, $J^h_{\mathrm{H_2O}}$ for fluxes from the extracellular space to the nearby healthy tissue.

The interstitium is composed mainly of collagen fiber bundles and proteoglycan filaments. The collagen fiber bundles are strong and provide significant resistance to large changes in the interstitial volume (Guyton and Hall 1996). We incorporate this aspect of interstitial matrix behavior by including a linear restoring force $c_1 \cdot ({V_e}^\infty - V_e)$ in the expression below for the term $J^h_{\mathrm{H_2O}}$ which appears in Equation(11). Here ${V_e}^\infty$ is the normal volume of the interstitial space. Also, the total volume (cells and interstitium) cannot grow without limit because of the presence of neighboring cells. We model this by including another elastic force $c_2 \cdot (V_T^\infty - V_i - V_e)$ in $J^h_{\mathrm{H_2O}}$ in equation (11).

$$J^h_{\mathrm{H_2O}} = -L^{eh}_p\left(c_1 \cdot ({V_e}^\infty - V_e) + c_2 \cdot (V_T^\infty - V_i - V_e)\right). \quad (12)$$

where V_T^∞ is the normal total volume of the intracellular and extracellular spaces. Because of the $J^h_{\mathrm{H_2O}}$ term in Equation(11), the total volume $V_i + V_e$ can change by an amount different from

the time-integral of the flux $J^v_{\mathrm{H_2O}}$ between the capillary and interstitium, allowing for volume exchange with the nearby healthy tissue. This fluid exchange is limited by the elastic force terms just described.

The ionic flux between the extracellular space in the damaged tissue and the surrounding normal tissue is modeled by

$$J^h_j = P^h \cdot \alpha_j \cdot \left(\frac{[C_j]^\infty_e - [C_j]_e \exp(\alpha_j)}{1 - \exp(\alpha_j)} \right), \tag{13}$$

where $\alpha_j = (J^h_{\mathrm{H_2O}})/(P^h) - (z_j F)/(RT) \cdot \delta_{eh}$. This flux formula accounts for convective ionic transport in addition to transport due to electrochemical potential differences. Here, C_j denotes the concentration of one of the ions (Na^+, K^+, Cl^-) and z_j is the corresponding ionic valence. The quantity δ_{eh} denotes the voltage difference between the damaged and healthy tissue. The parameter P^h is proportional to the ion diffusion coefficient and the surface area for exchange between the two regions. The detailed derivation of this flux formula is given in Appendix A.

Finally, we consider the capillary compartment which we assume is in Donnan equilibrium with the extracellular compartment. Q_a is the flow rate of the arterial blood and Q_v is the flow rate of the capillary. The extracellular voltage δ_e is the voltage with the reference voltage being that in the capillary compartment. The Donnan equilibrium arises when two spaces containing electrolyte are in equilibrium, and one or both of the spaces contain charged species that cannot exchange between the spaces. In our case, both the extracellular and capillary compartments contain charged protein as well as permeable solutes (Na^+, K^+, Cl^-). It is reasonable to assume that these compartments are in equilibrium because of the high permeability of the capillary wall to water and small ions (Guyton and Hall 1996). Donnan equilibrium is not established between the intracellular and extracellular spaces because of the action of the energy-consuming Na-K-ATPase pump in the cell membrane which maintains cell homeostasis. The equations for the capillary

compartment are:

$$0 = \delta_e - \delta_{Na}^{ev}, \tag{14}$$

$$0 = \delta_e - \delta_K^{ev}, \tag{15}$$

$$0 = \delta_e + \delta_{Cl}^{ev}, \tag{16}$$

$$0 = [Na^+]_v + [K^+]_v - [Cl^-]_v - z_v[Pr]_v, \tag{17}$$

$$0 = (\Pi_e - \Pi_v) \tag{18}$$

$$Q_v[\mathrm{Na}^+]_v = Q_a[\mathrm{Na}^+]_a + J_{\mathrm{Na}}^v, \tag{19}$$

$$Q_v[\mathrm{K}^+]_v = Q_a[\mathrm{K}^+]_a + J_{\mathrm{K}}^v, \tag{20}$$

$$Q_v[\mathrm{Cl}^-]_v = Q_a[\mathrm{Cl}^-]_a + J_{\mathrm{Cl}}^v, \tag{21}$$

$$Q_v[Pr]_v = Q_a[Pr]_a, \tag{22}$$

$$Q_v = Q_a + J_{\mathrm{H_2O}}^v. \tag{23}$$

In the above, $\delta_{\mathrm{S}}^{ev} = (RT)/(zF)\ln\left([\mathrm{S}]_v/[\mathrm{S}]_e\right)$ is the Nernst potential generated by differences in the concentration of ion S across the capillary wall. In Equation(18), Π_v is the osmotic pressure in the capillary space:

$$\Pi_v = \left([Na^+]_v + [K^+]_v + [Cl^-]_v + [Pr]_v\right).$$

Finally, to preserve the overall electrical neutrality of our system, we require that

$$0 = J_{\mathrm{Na}}^h + J_{\mathrm{K}}^h - J_{\mathrm{Cl}}^h. \tag{24}$$

In Equations(1)–(3), g_{Na}, g_{K} and g_{Cl} denote membrane conductances. The sodium and potassium conductances include the contributions from channels regulated by voltage-dependent gates. To describe these we use the voltage-dependent steady-state gating variables $m_\infty(\delta)$, $h_\infty(\delta)$, and $n_\infty(\delta)$ from the Hodgkin-Huxley model (Hodgkin and Huxley 1952). We use steady state gating variables instead of time-dependent gating variables because we are looking at the phenomena on a time scale (minutes) that is slow compared to action potentials.

The leak current of the original Hodgkin-Huxley model is a combination of a sodium background current, a potassium background current and a chloride current having constant conductances. Therefore, in equations (1), (2), (7), and (8) of our full model, the sodium and potassium conductances g_{Na} and g_{K} are defined by:

$$g_{\mathrm{Na}} \;=\; g^b_{\mathrm{Na}} + \overline{g_{\mathrm{Na}}} \cdot m_\infty(\delta)^3 \cdot h_\infty(\delta), \tag{25}$$

and

$$g_{\mathrm{K}} \;=\; g^b_{\mathrm{K}} + \overline{g_{\mathrm{K}}} \cdot n_\infty(\delta)^4. \tag{26}$$

Here

$$m_\infty = \frac{A_m}{A_m + B_m},\ h_\infty = \frac{A_h}{A_h + B_h} \text{ and } n_\infty = \frac{A_n}{A_n + B_n}\,;$$

$$\begin{aligned}
A_m &= \frac{0.1(25 - \delta + \delta_{eq})}{\exp\left(0.1(25 - \delta + \delta_{eq})\right) - 1.0},\\
B_m &= 4.0 \exp\left(\frac{-\delta + \delta_{eq}}{18.0}\right),\\
A_h &= 0.07 \exp\left(0.05(-\delta + \delta_{eq})\right),\\
B_h &= \frac{1.0}{\exp\left(0.1(30 - \delta + \delta_{eq})\right) + 1.0},\\
A_n &= \frac{0.01(10 - \delta + \delta_{eq})}{\exp\left(0.1(10 - \delta + \delta_{eq})\right) - 1.0},\\
B_n &= 0.125 \exp\left(\frac{-\delta + \delta_{eq}}{80}\right),
\end{aligned}$$

$\delta = \delta_i - \delta_e$, and $\delta_{eq} = -70$ mV is the resting potential in the Hodgkin-Huxley equations. g_{Cl} is constant as are the background conductances g^b_{Na} and g^b_{K}.

Using literature values (see Appendix B) for the normal pump rate, resting voltage, volumes, and ionic concentrations, we solve equations (1) and (2) to determine the total resting conductances g_{Na} and g_{K}, respectively. Next we need to find reasonable values for the coefficients of the voltage-dependent conductances $\overline{g_{\mathrm{Na}}}$ and $\overline{g_{\mathrm{K}}}$. We choose them to give an action potential with a shape and peak similar to that of the Hodgkin-Huxely model when we allow the gating variables to be time-dependent. Finally, we set δ to its resting value in equations (25) and (26) to determine values of g^b_{Na} and g^b_{K}, respectively. Later we show results for different values of g_{Cl}.

Our model consists of 21 equations and 20 unknowns:

$[Na^+]_i,\ [K^+]_i,\ [Cl^-]_i,\ V_i,\ \delta_i$ (in the intracellular compartment)

$[Na^+]_e,\ [K^+]_e,\ [Cl^-]_e,\ V_e,\ \delta_e$ (in the extracellular compartment)

$[Na^+]_v,\ [K^+]_v,\ [Cl^-]_v,\ [Pr]_v,\ Q_v$ (in capillary)

$J^v_{\mathrm{Na}},\ J^v_{\mathrm{K}},\ J^v_{\mathrm{Cl}},\ J^v_{\mathrm{H_2O}}$ (flux from extracellular to capillary)

δ_{eh} (voltage difference between damaged and normal extracellular spaces)

However, this system of equations is not overdetermined, since one of equation (4) or equation (10) is a consequence of the other equations. This can be demonstrated algebraically and is a direct consequence of our enforcing overall electroneutrality and our tracking ion movements between compartments.

For modeling ischemia and hypoxia we assume that the Na-K-ATPase rate decreases with time in a prescribed way. We use the decay function $a(t) = (0.35)^{(t/15)}$ fit to Jennings and Reimer (1991)'s ATP data (see Figure 2) as a surrogate for the decay in the pump rate. The pump rate's decay actually depends on the decrease in ATP just below the cell membrane, and other factors including the decrease in intracellular pH during ischemia. The timecourse of these factors is not known and we use $a(t)$ as a crude substitute. We use as pump rate the formula used in Luo and Rudy (1991) multiplied by our decay function $a(t)$:

$$P = a(t) \cdot P_{\max} \cdot f_{\mathrm{NaK}} \cdot \left(\frac{1}{1 + \left(\frac{K_{m,\mathrm{Na}_i}}{[\mathrm{Na}^+]_i} \right)^{1.5}} \right) \cdot \left(\frac{[\mathrm{K}^+]_e}{(K_{m,\mathrm{K}_e} + [\mathrm{K}^+]_e)} \right),$$

where

$$f_{\mathrm{NaK}} = \frac{1}{1 + 0.1245 \exp(\frac{-0.1\delta \cdot F}{RT}) + 0.0365 \cdot 7 \cdot \exp(\frac{-\delta \cdot F}{RT})(\exp(\frac{[\mathrm{Na}^+]_e}{67.3}) - 1)}.$$

For ischemia, we make the additional assumption that $Q_a = 0$ to reflect cessation of flow into the arterial side of the tissue's capillary bed.

Discrete Solution of Model Equations

The model equations are a mix of ordinary differential equations and algebraic equations. To solve them, time is broken into discrete timesteps of length Δt, and approximate solutions to

the equations are determined at times $t_n = n\Delta t$ for $n = 1, 2, ...$ For any variable, its value at time t_n is indicated by a superscript n. We have found that computational results are very sensitive to enforcing electroneutrality exactly in each compartment and so we take special care in determining the voltages so that these constraints hold. To determine values of the variables at time t_{n+1} from the known values at time t_n we proceed as follows:

To enforce the Donnan equilibrium across the capillary wall, we use Eqs(14-16) to express the unknowns $[Na^+]_v^{n+1}$, $[K^+]_v^{n+1}$, and $[Cl^-]_v^{n+1}$, in terms of the known values $[Na^+]_e^n$, $[K^+]_e^n$, and $[Cl^-]_e^n$, and the unknown transcapillary voltage δ_e^{n+1}. These expressions are substituted into (17) to express $[Pr]_v$ in terms of known values and the unknown δ_e^{n+1}. Finally all of these expressions are substituted into (18) to yield a quadratic equation for $\exp(\delta_e^{n+1}F/RT)$. In practice this quadratic equation has always had one positive solution, from which we determine δ_e^{n+1}. Then $[Na^+]_v^{n+1}$, $[K^+]_v^{n+1}$, $[Cl^-]_v^{n+1}$, and $[Pr]_v$ are calculated from Eqs(14)-(16). Q_v^{n+1} is then determined from Eq(23), and $J_{Na}^{v,n+1}$, $J_K^{v,n+1}$, $J_{Cl}^{v,n+1}$, and $J_{H_2O}^{v,n+1}$ are determined from Eqs(19-21,23) respectively. The new values $J_{H_2O}^{h,n+1}$, $J_{Na}^{h,n+1}$, and $J_K^{h,n+1}$ are then calculated from Eqs(12-13) using values of the extracellular concentrations, extracellular volume, and intracellular volume from time t_n and the newly calculated extracellular voltage δ_e^{n+1}. We set $J_{Cl}^{h,n+1} = -J_{Na}^{h,n+1} - J_K^{h,n+1}$ to satisfy Eq(24).

It remains to determine new values of the intra- and extracellular variables. The new transmembrane voltage $\delta^{n+1} = \delta_i^{n+1} - \delta_e^{n+1}$ is determined from the equation which results upon differentiating the intracellular electroneutrality equation (4) and substituting into it the flux expressions from Eqs(1-3). In evaluating the conductances and the equilibrium potentials in this expression, the voltage and concentrations from time t_n are used. Once, δ^{n+1} has been calculated, new values of the intra- and extracellular ion concentrations and volumes are determined using a simple explicit time-stepping approximation to the differential equations (1-3,5-9,11).

Long Term Stability of Model

A surprising obstacle to studying models of the type we propose here was the difficulty we encountered in formulating models that display long-term stability even under conditions corresponding to normal healthy tissue. By long-term stability we mean the following. Suppose

we calculate a steady state solution to the model's equations under healthy conditions, and then we perturb the variables a small amount from this solution, and solve the time-dependent equations. If the solution returns to the steady state solution or remains close to it, we call the steady state long-term stable. If one or more of the model variables move far away from their steady state values and remain far away, we call the steady state long-term unstable. Clearly long-term stability under healthy conditions is a necessary feature of a model if we propose to use it to study how unhealthy conditions affect the variables. Early versions of our models were long-term unstable, and we traced the problem to the absence of a sodium background (leak) conductance. In Figure(4), we illustrate the problem with a calculation using the model presented in this paper. With g^b_{Na} set to the value given in Appendix B, all variables remained very close to their steady state values even for simulations of over 1000 minutes. With $g^b_{\mathrm{Na}} = 0$, a strong instability occurred. One manifestation of this is that the intracellular sodium concentration $[Na^+]_i$ dropped sharply from its steady state value over a 50 minute simulation. Over the same time period, $[K^+]_i$ increased from 140 mM to about 151 mM, $[Cl^-]_i$ decreased from its rest value of just under 5 mM to a little under 4 mM while intra- and extracellular volumes changed very little.

The model we have developed in this paper is a modification of a Hodgkin-Huxley model to include ion pumps and volume regulation. These modifications were made in such a way that the steady state of the system was not changed. However, as just seen, the stability of the steady state can be strongly affected by these modifications. In all the studies reported in this paper, we made certain that the model showed long-term stability under healthy tissue conditions. We encountered similar stability problems in the absence of a sodium leak conductance with modifications of other ionic models including Beeler-Reuter (Beeler and Reuter 1977), Luo-Rudy I (Luo and Rudy 1991), and DiFrancesco-Noble (DiFrancesco and Noble 1985). We note that similar stability problems have been alluded to by Courtemanche et al. (1998) and Wilders et al. (1991).

Coupling to Healthy Tissue

A novel feature of our model is the provision for elastic resistance to changes in the volume of

the extracellular and total volumes of the damaged tissue. The resistance to compression of the extracellular space takes the form of a swelling pressure that draws fluid into this tissue from the surrounding tissue, and is intended to reflect the gel character of the interstitial material. The need for coupling of water and solute between the damaged and normal tissues is illustrated in Figure(5) which shows $[K^+]_e$ and V_e for the case of no coupling (achieved by setting $c_1 = c_2 = P^h = 0$). We see that the extracellular space shrinks by almost 80% and that the extracellular potassium concentration reaches levels far beyond any reported experimentally. Comparing these results with those that allow coupling (see Figure 9 for $[K^+]_e$ and Figure 13 for V_e) shows that the timecourse of $[K^+]_e$ and V_e is very similar for the first 15 minutes of the simulation but then diverge sharply as V_e continues to decline sharply in the absence of coupling, and consequently, the extracellular potassium concentration shows another dramatic rise. Both the size of the decrease in extracellular volume and the extent of increase in extracellular potassium are far greater than any reported experimentally. In contrast, with coupling of the ischemic and normal tissues, the extracellular volume and extracellular potassium concentrations level off, as the fluxes of water and potassium across the cell membrane are matched by their flux between the normal and ischemic regions. For the remainder of this paper, all simulations were performed with coupling to healthy tissue.

Parameter Values

Our model describes the behavior of a collection of cells and their interactions with their surroundings during ischemia and hypoxia. The number of cells considered does not enter explicitly into our modeling and calculations since most quantities simply scale with the number of cells. For example, the total intracellular volume for N identical cells is simply $N \cdot V_i$ where V_i is the intracellular volume of a single cell. In our report of parameter values for volume, total number of ions or proteins, volume flux of water, and number flux of ions, we express quantities in the appropriate units *per cell*. Several of the model's parameters may scale in a non-trivial way with the number of cells considered or the size of the region they occupy. This is true in particular of the parameters, L_p^{eh}, P^h, c_1, and c_2, that characterize the coupling between the damaged tissue and the surrounding healthy tissue. Our modeling of this coupling is very simplistic and does not

permit a clear determination of how these parameters should scale. Instead we consider below how variations in these parameters' values affect the model's behavior. We note that L_p^{eh}, c_1, and c_2, are not independent parameters in the model as only the products $L_p^{eh} \cdot c_1$ and $L_p^{eh} \cdot c_2$ appear in Equation(12). These products have dimensions of inverse time, so we define time constants $\tau_1 = 1/(L_p^{eh} \cdot c_1)$ and $\tau_2 = 1/(L_p^{eh} \cdot c_2)$ so that Equation (12) can be written in the alternative form:

$$J^h_{\mathrm{H_2O}} \;=\; -\left(\frac{1}{\tau_1} \cdot (V_e{}^{\infty} - V_e) \;+ \frac{1}{\tau_2} \cdot (V_T^{\infty} - V_i - V_e)\right).$$

Below we report the model's behavior in terms of these time constants:

RESULTS

We begin by exploring the differences in behavior of our model under ischemic and hypoxic conditions. A comparison of the model's predicted changes in $[K^+]_e$ during ischemia and hypoxia are given in the left panel of Figure 6. The right panel shows the experimental data for hypoxia from Yan et al. (1993) and for ischemia from Hansen (1978). The ischemia data is for brain tissue and we see that our computational results capture the main features observed by Hansen – a delay during which $[K^+]_e$ rises slowly, followed by a very rapid increase in $[K^+]_e$ beginning when $[K^+]_e$ reaches about 10 mM. Below we explain what we believe is the origin of this biphasic behavior. Our results for hypoxia are quite similar to those of Yan and coworkers, namely, that there is very little change in $[K^+]_e$.

The main reason for this observed difference between hypoxia and ischemia is that during hypoxia there is a washout of potassium from the extracellular space. Therefore, accumulation of $[K^+]_e$ is negligible in hypoxia, while it is very noticeable in ischemia. In both situations, the lack of oxygen in the cell leads to a decrease in activity of the Na-K-ATPase pump. In normal tissue, $[K^+]_i = 140$ mM is much bigger than $[K^+]_e = 5.4$ mM. Without an active Na-K-ATPase pump, $[K^+]_e$ increases since the loss of potassium from the cell due to this concentration difference is not balanced by restoration of intracellular potassium by the pump. This happens in both ischemia and hypoxia. In hypoxia, however, the K^+ lost from the cell to the extracellular space does not accumulate because it is continuously washed away. This can be seen in Figure 7 which shows water flux ($J^v_{\mathrm{H_2O}}$) and ionic fluxes ($J^v_{\mathrm{Na}},\ J^v_{\mathrm{K}},\ J^v_{\mathrm{Cl}}$) with respect to time.

Rapid rise in $[K^+]_e$ and the nonlinearity of g_{Na}

In our calculations, the nonlinearity of the sodium conductance plays a major role in extracellular potassium accumulation during ischemia. Recall that we assume that $g_{\mathrm{Na}} = g^b_{\mathrm{Na}} + \overline{g_{\mathrm{Na}}} \cdot m_\infty(\delta)^3 \cdot h_\infty(\delta)$ where g^b_{Na} and $\overline{g_{\mathrm{Na}}}$ are constants and $m_\infty(\delta)$ and $h_\infty(\delta)$ are Hodgkin-Huxley type gating variables for sodium channel opening and closing respectively. Figure 8 shows two calculations, in one of which $g^b_{\mathrm{Na}} = 3.314 \cdot 10^{-5} \frac{\mathrm{mcoul}}{\mathrm{volt \cdot min}}$ and $\overline{g_{\mathrm{Na}}} = 3.689 \cdot 10^{-2} \frac{\mathrm{mcoul}}{\mathrm{volt \cdot min}}$ so that before the onset of ischemia $g_{\mathrm{Na}} = 3.326 \cdot 10^{-5} \frac{\mathrm{mcoul}}{\mathrm{volt \cdot min}}$; and in the other of which $g^b_{\mathrm{Na}} = 3.326 \cdot 10^{-5} \frac{\mathrm{mcoul}}{\mathrm{volt \cdot min}}$ and $\overline{g_{\mathrm{Na}}} = 0.0 \frac{\mathrm{mcoul}}{\mathrm{volt \cdot min}}$ (so that sodium conductance is constant, independent of voltage). Only

the calculation with the nonlinear sodium gating shows a rapid rise in $[\mathrm{K}^+]_e$ following the onset of ischemia (see Figure 8, bottom panel).

To understand this, consider the differential equation (8) for total extracellular potassium

$$\frac{d(V_e[K^+]_e)}{dt} = \frac{g_{\mathrm{K}}}{F}\,(\delta_i \;-\; \delta_e \;-\; \delta_K) - 2P - J^v_{\mathrm{K}} - J^h_{\mathrm{K}}.$$

Since the arterial flow Q_a into the capillary is zero during ischemia, the transcapillary flux of potassium $J^v_{\mathrm{K}} = 0$. A rapid efflux of potassium can only be due to transmembrane flux; and the driving force for this efflux is $\delta - \delta_K$ where $\delta = \delta_i - \delta_e$. It follows from our electroneutrality assumption (equation (4)) and the flux equations (1)–(3) that

$$\delta \;-\; \delta_K = \frac{g_{\mathrm{Na}}}{g_{\mathrm{tot}}}(\delta_{Na} \;-\; \delta_K) \;+\; \frac{g_{\mathrm{Cl}}}{g_{\mathrm{tot}}}(\delta_{Cl} \;-\; \delta_K) - \frac{P\cdot F}{g_{\mathrm{tot}}}, \tag{27}$$

where $g_{\mathrm{tot}} = g_{\mathrm{Na}} + g_{\mathrm{K}} + g_{\mathrm{Cl}}$. As the pump rate decreases during ischemia, the no-longer fully balanced electro-chemical potential gradients of Na^+ and K^+ lead to membrane depolarization. Because of the behavior of the gating variables $m_\infty(\delta)$ and $h_\infty(\delta)$, the curve $g_{\mathrm{Na}}/g_{\mathrm{tot}}$ is bell-shaped (see Figure 8, top left panel) which gives a similar hump to the term $(g_{\mathrm{Na}}/g_{\mathrm{tot}})(\delta_{Na} - \delta_K)$ and in fact to the entire driving force (see Figure 8, top right panel) for all values of g_{Cl} that we considered. The decrease of pump rate P with time means that the third term in equation (27) becomes less negative which also increases the driving force but on a slower time scale. The term $(g_{\mathrm{Cl}}/g_{\mathrm{tot}})(\delta_{Cl} - \delta_K)$ adds to the driving force when $\delta_{Cl} > \delta_K$, which is true initially, but reduces the driving force, even to the extent of reversing its sign later in the simulations. This is discussed further below. The absence of nonlinearity in g_{Na} eliminates the hump in the driving force (see Figure 8, top right panel) and in this case $[K^+]_e$ rises only slowly.

The increase of g_{K} with δ reinforces the effect of the hump of the driving force, but is not necessary for a rapid increase in $[K^+]_e$. To see whether nonlinearity of g_{K} affects a rapid increase in $[K^+]_e$, we follow the same procedure as for g_{Na}. Recall that we assume that $g_{\mathrm{K}} = g^b_{\mathrm{K}} + \overline{g_{\mathrm{K}}}\, n_\infty(\delta)$ where g^b_{K} and $\overline{g_{\mathrm{K}}}$ are constants and $n_\infty(\delta)$ is the Hodgkin-Huxley type gating variable for potassium. Figure 9 shows the results of two calculations, in one of which $g^b_{\mathrm{K}} = 8.332\cdot 10^{-4}\frac{\mathrm{mcoul}}{\mathrm{volt}\cdot\mathrm{min}}$ and $\overline{g_{\mathrm{K}}} = 1.283\cdot 10^{-2}\frac{\mathrm{mcoul}}{\mathrm{volt}\cdot\mathrm{min}}$ so that before the onset of ischemia $g_{\mathrm{K}} = 8.469\cdot 10^{-4}\frac{\mathrm{mcoul}}{\mathrm{volt}\cdot\mathrm{min}}$; and in the other of which $g^b_{\mathrm{K}} = 8.469\cdot 10^{-4}\frac{\mathrm{mcoul}}{\mathrm{volt}\cdot\mathrm{min}}$ and $\overline{g_{\mathrm{K}}} = 0.0\frac{\mathrm{mcoul}}{\mathrm{volt}\cdot\mathrm{min}}$.

In the second calculation, the total potassium conductance under normal (nonischemic) conditions is the same as in the first, but the nonlinear voltage-dependent contribution is absent. Total g_{K} is larger, however the driving force $(\delta - \delta_K)$ is smaller, so that overall there is little difference in $[K^+]_e$ for the two cases.

Plateau behavior of $[K^+]_e$ during ischemia

The set-up of our model is based on regional ischemia (the existence of an ischemic region and a surrounding undamaged region) or ischemic tissue bathed in an experimentally controlled solution. The results of our simulations suggest that the potassium flux between the two regions influences the extent to which a plateau in $[K^+]_e$ is seen. By plateau we mean the phase after the rapid rise in which $[K^+]_e$ is slowly decreasing (see Figure 10, bottom panel).

Based on our calculations, it is suggested that during regional ischemia, the plateau is at least in part due to a balance between continuous removal of potassium from ischemic tissue and continuous potassium loss from ischemic myocytes. The top left panel of Figure 10 describes numerical experiments with different values of the coupling parameter P^h. Recall that larger P^h corresponds to easier movement of ions between the damaged and normal extracellular spaces. For bigger values of P^h, $[K^+]_e$ has a more notable plateau with a lower peak; There is also a longer time delay before the rapid rise phase of extracellular potassium. This is because it takes longer for the transmembrane voltage to rise enough to substantially change the sodium conductance. As the top right panel shows, there is a much larger potassium flux between the two extracellular regions when P^h is larger. The bottom panel of Figure 10 shows the behavior of $[K^+]_e$ seen during ischemia in cardiac cells (Hill and Gettes 1980); $[K^+]_e$ has obvious triphasic behavior consisting of a rapid rise (after an initial lag), a 'plateau' during which $[K^+]_e$ decreases a little, and a second rise that is much slower than in the first phase. It also shows that $[K^+]_e$ behaves differently in the central core of the ischemic tissue and in the border zone tissue on the edge of the ischemic region. The central core shows an earlier rapid rise and a higher plateau than in the border zone. Our calculations agree qualitatively with these latter observations if one identifies larger P^h with being in the border zone and therefore able to exchange ions more readily with the normal tissue.

The Pump's Role in the Dynamics of $[K^+]_e$ during Ischemia

The left panel of Figure 11 shows three simulations in which the rates of decrease of the Na-K-ATPase pump rate differ. If the pump is instantly made inactive, $[K^+]_e$ increases without an initial lag, while a reduction in maximal pump rate in proportion to the reported reduction (Jennings and Reimer 1991) of [ATP] leads to a significant lag. The faster the reduction in pump rate, the shorter the lag.

Hansen (1978) studied ischemia in rat brains from rats with different levels of blood glucose (hyperglycemic; normal=control; hypoglycemic) before ischemia was induced. It is reasonable to assume that cell ATP levels before ischemia were higher, equal to, or lower than normal levels under these respective conditions. The right panel of Figure 11 shows Hansen's $[K^+]_e$ data from ischemic tissue of hypoglycemic and normal rats. We see that the initial lag was much shorter for the hypoglycemic rats; and that for both populations, the lag was followed by a very rapid rise; and then a much slower rise. The rate of increase during the rapid rise for the different pre-ischemia glucose levels was very similar. Again our simulations are in qualitative agreement with these observations; $[K^+]_e$ levels at the onset of and after the rapid rise are in agreement with Hansen's data, but, as before, there is longer delay before this rise in our simulations than in the experiments.

Comparison of $[\mathrm{Na}^+]_i$ Increase in Ischemia and Hypoxia

In normal tissue, $[Na^+]_i = 11.2$ mM which is much smaller than $[Na^+]_e = 140$ mM. As the Na-K-ATPase pump rate decreases during ischemia or hypoxia, there is a net influx of sodium because the influx of sodium due to this concentration gradient is not balanced by restoration of extracellular sodium by the pump. For the first 12 minutes or so (see Figure 12), the increase in $[Na^+]_i$ is very similar for ischemia and hypoxia, but then, in the ischemia case, the sodium conductance increases substantially, and this leads to a much more rapid rise in $[Na^+]_i$ during the interval 12 to 18 minutes.

The $[Na^+]_i$ increases more and more slowly after this. The explanation for this last phase is that the decreased pump rate leads to a net increase in osmolarities inside the cell (as discussed below). As a consequence, the cell swells (see Figure 13 left) and so the rate of increase of

$[Na^+]_i$ slows although the sodium influx continues. In hypoxia, although the Na^+ conductance increases significantly, the volume changes little, so that the $[Na^+]_i$ curve increases steadily without showing the three phases of slow/fast/slow increase.

Intra- and Extracellular Volume Behavior

Our calculations in the case of ischemia show an increase of intracellular volume V_i by 6% in 15 minutes, and 26% in 30 minutes (Figure 13a), while V_i changes much less during hypoxia. This difference is similar to that reported by Jennings and Reimer (1991). Fiolet et al. (1993) report cells swelling by about 20% during 30 minutes of ischemia, similar to what we see. With regard to the extracellular volume, Yan et al. (1996) report a 14–16% decrease of extracellular volume V_e during 10 minutes of ischemia, and a 30% decrease in 20 minutes (see Figure 13b), while Fiolet (Fiolet et al. 1993) report a 14% decrease and a 25% decrease during 8–15 minutes and 30 minutes of ischemia respectively. Our simulations show a similar decrease, 16% in 15 minutes, and 21% in 20 minutes (see Figure 13c), although the time course of the decrease is different than that seen in the experimental data.

Cell swelling in our model is initiated by the reduction in pump rate. An active pump removes three sodium ions for every two potassium ions brought into the cell, and so failure of the pump changes the osmotic balance between the intra- and extracellular spaces and causes the cell to swell. As Figure 13a shows, the rate of increase in V_i for ischemia is somewhat greater than for hypoxia for about 12 minutes, and then becomes substantially larger. This change coincides with the voltage-induced change in g_{Na} which allows a rapid rise in $[Na^+]_i$. During hypoxia, the extracellular concentration of potassium changes little and so the transmembrane voltage does not increase sufficiently to trigger this rapid influx of sodium. A second factor which influences the different intracellular volume responses in ischemia and hypoxia has to do with which other ions move across the cell membrane to preserve intracellular electroneutrality in the face of the increase of intracellular sodium. The possibilities are an influx of chloride ions which augments the osmotic effect of the sodium influx, or an efflux of potassium which decreases the osmotic effect of the sodium. During ischemia, potassium accumulates in the extracellular space making it increasingly difficult for more potassium to leave the cell, and leading to a larger influx of

chloride. In fact, as we show later, the larger the chloride conductance $g_{\rm Cl}$, the greater the influx of chloride, the smaller the efflux of potassium, and the greater the change in V_i. During hypoxia, there is very little change in $[K^+]_e$ because of continued exchange with the capillary, the efflux of potassium from the cell almost exactly balances the sodium influx, and $[Cl^-]_i$ remains almost constant, so that the osmotic force is greatly lessened in comparison to what happens in the case of ischemia.

Effect of Elastic Time Constants τ_1 and τ_2

Figure 14 shows three simulations with different pairs of values for the time constants τ_1 and τ_2. For time constants short compared with the duration of the simulation, V_e changes an amount in approximate agreement with experimental observations and these are the time constants used in all experiments unless otherwise noted. For significantly less stiff elastic behavior and therefore longer time constants, the qualitative behavior of the three curves for $[K^+]_e$, $J^h_{\rm K}$ and V_e are similar, but the change in extracellular volume is unacceptably large. Figure 14 also shows that for all three sets of τ_1 and τ_2, different values of the parameter P^h have similar effects.

Chloride Conductance $g_{\rm Cl}$:

Different types of cells have significantly different chloride conductance $g_{\rm Cl}$. In particular, this conductance is much larger for nerve cells than for cardiac cells (Hwang and Gadsby 1994). Figure 15 shows how different values of $g_{\rm Cl}$ affect the solution of our model equations.

We observe (Figure 15, top left) that as $g_{\rm Cl}$ increases from 0.0301 to 0.225 $\frac{\rm mS}{\rm cm^2}$, the time lag before the beginning of a rapid rise in extracellular potassium concentration increases, and the peak decreases from 55 mM to 45 mM. To understand how $[K^+]_e = (V_e[K^+]_e)/V_e$ changes, it is useful to look at how the total amount of extracellular potassium $(V_e[K^+]_e)$ and the extracellular volume V_e change. By adding equations (2) and (8) and noting that $J^v_{\rm K} = 0$ in ischemia, we find

$$\frac{d(V_e[K^+]_e)}{dt} = -\frac{d(V_i[K^+]_i)}{dt} - J^h_{\rm K}. \tag{28}$$

The first term on the right side is the rate potassium crosses the cell membrane and the second is the rate at which potassium moves between the damaged and normal interstitial regions. V_e is governed by equation (11) with $J^v_{\rm H_2O} = 0$. The effect of different $g_{\rm Cl}$ on the transmembrane

potassium flux is shown in Figure 15, middle right. The sharp spike in the flux occurs later and has a lower peak for the larger chloride conductance. Recall that slowdown of the Na-K-ATPase pump leads directly to a net increase of intracellular osmolarity and charge, and that the latter is balanced by a combination of potassium efflux and chloride influx which, respectively, reduce or increase intracellular osmolarity. The larger g_{Cl}, the smaller is the potassium efflux portion of the balance for any particular transmembrane potential, and the slower is the potassium accumulation in the extracellular space. The slower increase in $[K^+]_e$ leads to a slower change in the potassium Nernst potential and transmembrane voltage, and therefore delays the increase in g_{Na} conductance that leads to the rapid rise in transmembrane potassium flux as described earlier. So larger g_{Cl} causes both a reduction in the potassium efflux and a delay in the rapid efflux phase. The result is a reduction in peak total extracellular potassium $V_e[K^+]_e$ by about 33%. The percent reduction in $[K^+]_e$ is significantly smaller than this because of the osmotic consequences of larger g_{Cl}, that is, the intracellular volume V_i is larger, and the extracellular volume V_e is smaller. The other term, J^h_{K}, in equation (28), responds to the level of $[K^+]_e$ (relative to the normal extracellular potassium concentration) so that J^h_{K} and the transmembrane potassium efflux are almost in balance after the spike in the efflux, and both the total extracellular potassium and its concentration are approximatedly constant in the period following the spike.

DISCUSSION

We have used an ionic model that permits changes in intracellular and extracellular ionic concentrations and volumes to explore the response of tissue to hypoxia and ischemia. The model also involves exchange of ions and water between the vascular system and between the extracellular space of the hypoxic/ischemic tissue and nearby normal healthy tissue. For both hypoxia and ischemia, the effectiveness of the Na-K-ATPase was assumed to decrease with time following a prescribed timecourse that we estimated from reports in the literature of [ATP] decline during ischemia. In addition, for ischemia we assumed that arterial flow to the tissue ceased.

Literature reports on the increase of the extracellular potassium concentration during ischemia show substantially different behavior for brain and cardiac tissue. For brain tissue, there is a slow rise in extracellular potassium to a level of about 10 mM at which point the $[K^+]_e$ increases much more rapidly to levels in the range 50-80 mM, and then plateaus.. For cardiac tissue, the initial rise to 10-12 mM is followed by a plateau phase in which $[K^+]_e$ changes little for 10-15 minutes.

The main result of this paper is a possible explanation for the time course of $[K^+]_e$ during ischemia in brain tissue, and an understanding of the reason that such a time course is not expected in the cardiac case. For neural tissue, the key observation is the shape of the functional dependence of steady-state sodium conductance on transmembrane voltage. As shown in Figure(16), there is a range of voltages for which both the m and h gates are open. The basic mechanism which our model shows can account qualitatively for the behavior of $[K^+]_e$ during neural ischemia is the following: As the effectiveness of the Na-K-ATPase pump decreases, $[K^+]_e$ and $[Na^+]_i$ gradually increase and this causes a gradual depolarization. Because the potassium conductance is significantly larger than that of sodium, most of this depolarization is a consequence of the change in the potassium Nernst potential, and the membrane potential roughly tracks the potassium Nernst potential. When $[K^+]_e$ reaches a level of about 10 mM, the membrane has depolarized to an extent that the nonlinearity in the sodium conductance becomes significant. Sodium rapidly enters the intracellular space, the membrane potential rapidly depolarizes (on this time scale), and this provides a large driving force (see Figure 8 top right) pushing potassium out

of the cells into the interstitium. In response to the rapid depolarization, the sodium conductance drops so that the potassium conductance is again dominant, the transmembrane potential approaches the new potassium Nernst potential, and the efflux of potassium slows considerably until it is matched by the movement of potassium from the ischemic tissue to nearby healthy tissue. In cardiac ion models, the steady-state sodium conductance has a very different dependence on voltage. For example, in the Beeler-Reuter and Luo-Rudy I models, the opening of the sodium activation gates and the closing of the sodium inactivation gates are shifted in their dependence on voltage in such a way that there is only a small interval of voltages in which both activation and inactivation gates are open, and the relative magnitude of the nonlinear sodium conductance to the background conductance is only about 5% compared to an over 100% increase in sodium conductance in the nerve model (see Figure 8 top left). Thus we do not expect to see a rapid turning on of potassium efflux in cardiac tissue, and this is consistent with experimental observations. We note that our model's predicted rise in $[K^+]_e$ after 10 minutes of ischemia in the absence of a nonlinearity in the sodium conductance (see Figure 8 bottom) is comparable to those reported in cardiac tissue after 5-10 minutes of ischemia. In this case, the model's $[K^+]_e$ continues to rise gradually rather than leveling off at a concentration of 10-12 mM. This may be because, in the model, the rate of efflux of potassium has not equilibrated with the rate of transport of potassium from the damaged to the surrounding healthy tissue.

The model we have proposed has many limitations, among which are the assumption that the ischemic zone consists of homogeneous cells surrounded by a homogeneous extracellular space. The mechanical response of the tissue to volume changes (through Equations (11) and (12)) and the coupling between damaged and normal tissue are also modeled in very simple ways, and this no doubt affects at least the quantitative behavior of the model. An improved, but also much more complicated, model would involve spatial variation in the degree of ischemia and in the transport of water and ions. Such a model would also explicitly have built in the size of the tissue considered, and then the degree of coupling between normal and damaged tissue would be a consequence of this size and the properties in each kind of tissue. In the context of the current model, the coupling parameter P^h is intended to reflect the average coupling between healthy

tissue and ischemic tissue where different points in the ischemic tissue are different distances from the healthy tissue. It is also intended to account for the small fraction of the total volume (the gaps between cells) through which the ions can move, and with other factors which might hinder ion transport. Estimates of effective diffusivities in other contexts, biological (Fogelson and Wang 1996) and industrial (Fogler 1986), suggest that it is reasonable to consider the small values of P^h that we examined in this paper. Another limitation is due to the unavailability of reliable data about the timecourse of the decline in effectiveness of the Na-K-ATPase pump. As indicated earlier, several factors may contribute to this decline including a reduction in the relevant pool of ATP, a change in pH, and a change in the concentrations of ions other than sodium and potassium. We have not sought to predict the rate of decline and to account for these different factors, but instead have used measured tissue ATP concentration during ischemia as a surrogate for this decline. This is clearly an approximation, and may contribute to the difference in time of onset of the rapid rise in $[K^+]_e$ between our simulations and Hansen's data from brain tissue.

Acknowledgments: The authors are grateful to Alex Kralios and Alan Weinstein for helpful discussions. This work was supported, in part, by NSF grant DMS-9805518 and a John Simon Guggenheim Memorial Foundation Fellowship to Fogelson and NSF grant DMS99-700876 to Keener.

Appendix A: Derivation of Ion Fluxes J_j^{eh}

We derive the ionic flux (Equation 13) between the damaged extracellular space (Region 1) and the surrounding normal tissue (Region 2) due to the combined effects of convection, and an electrochemical potential gradient. We imagine that the two regions are separated by a distance L and communicate with one another over a surface of area S. We consider how the ion concentration C_j varies in the interval $0 \leq x \leq L$, with the boundary conditions $c_j(0) = [C_j]_e$, and $c_j(L) = [C_j]_e^{\infty}$. Let $c_j(x) = [C_j](x)$ denote the concentration of ion j and $\delta(x)$ be the potential at location x. The ion flux is the sum of three terms

$$J_j^{eh}(x) = S\left\{u_{\mathrm{H_2O}}\, c_j(x) - \mu\left(\frac{z_j}{|z_j|}\right) c_j(x)\, \delta'(x) - D\, c_j'(x)\right\}. \tag{29}$$

due to convention, the electrical potential gradient, and the ion concentration gradient, respectively. A prime denotes a derivative with respect to x, In (29), $u_{\mathrm{H_2O}} = J^h_{\mathrm{H_2O}}/S$ is the average velocity of the water moving between the two compartments, D is the ion's diffusion coefficient, and $\mu = (|z_j|F)/(RT) \cdot D$ is the ion's mobility, that is, its velocity in a unit electric field. We make the constant field assumption so that $\delta' = ({\delta_e}^{\infty} - \delta_e)/L$, we assume that the steady state flux is constant $J(x) = J_o$ for all x, and seek to determine J_o consistent with the boundary values at $x = 0$ and L. We have the ordinary differential equation

$$S\left(-D\, c_j' + \Phi\, c_j\right) = J_o, \tag{30}$$

subject to the stated boundary conditions on c_j. Here, $\Phi = u_{\mathrm{H_2O}} - (z_j F)/(RT) \cdot D \cdot ({\delta_e}^{\infty} - \delta_e)/L$. Integrating (30) gives

$$[C_j](x) = \frac{J_o}{\Phi} + A\exp(\frac{\Phi\, x}{D}),$$

and imposing the boundary conditions determines A and J_o and yields

$$J_j^{eh} = P^h \alpha_j \left(\frac{[C_j]_e^{\infty} - [C_j]_e \exp(\alpha_j)}{1 - \exp(\alpha_j)}\right),$$

with $P^h = (SD)/L$ and $\alpha_j = J^h_{\mathrm{H_2O}}/P^h - (z_j F)/(RT)\,({\delta_e}^{\infty} - \delta_e)$ as claimed. A related derivation can be found in (Patlak et al. 1963).

Appendix B: Variables and Parameters

Table 1: **Steady State Values of Variables**

$[Na^+]_i$	Intracellular $[Na^+]$	11.2 mM	a
$[Na^+]_e$	Extracellular $[Na^+]$	140 mM	a
$[Na^+]_v$	Capillary $[Na^+]$	136.7 mM	b
$[K^+]_i$	Intracellular $[K^+]$	139 mM	a
$[K^+]_e$	Extracellular $[K^+]$	5.4 mM	a
$[K^+]_v$	Capillary $[K^+]$	5.27 mM	b
$[Cl^-]_i$	Intracellular $[Cl^-]$	4.95 mM	b
$[Cl^-]_e$	Extracellular $[Cl^-]$	110 mM	a
$[Cl^-]_v$	Capillary $[Cl^-]$	112.7 mM	b
V_i	Cell Volume	$3.80 \cdot 10^{-8}$ cm^3	d
V_e	Interstitial Volume	$9.50 \cdot 10^{-9}$ cm^3	d
$\delta_i - \delta_e$	Membrane Potential	-80 mV	a
$[Pr]_v$	Capillary protein concentration	1.45 mM	b
Q_v	Capillary flow	$3.6 \cdot 10^{-8}$ $\frac{\text{cm}^3}{\text{min}}$	d
$J^v_{\text{H}_2\text{O}}$	Water flux from extracellular to capillary	0.0 $\frac{\text{cm}^3}{\text{min}}$	c
J^v_{Na}	Na^+ flux from extracellular to capillary	0.0 $\frac{\text{cm}^3\,\text{mM}}{\text{min}}$	c
J^v_{K}	K^+ flux from extracellular to capillary	0.0 $\frac{\text{cm}^3\,\text{mM}}{\text{min}}$	c
J^v_{Cl}	Cl^- flux from extracellular to capillary	0.0 $\frac{\text{cm}^3\,\text{mM}}{\text{min}}$	c
$J^h_{\text{H}_2\text{O}}$	Water flux from damaged to healthy interstitium	0.0 $\frac{\text{cm}^3}{\text{min}}$	c
J^h_{Na}	Na^+ flux from damaged to healthy interstitium	0.0 $\frac{\text{cm}^3\,\text{mM}}{\text{min}}$	c
J^h_{K}	K^+ flux from damaged to healthy interstitium	0.0 $\frac{\text{cm}^3\,\text{mM}}{\text{min}}$	c
J^h_{Cl}	Cl^- flux from damaged to healthy interstitium	0.0 $\frac{\text{cm}^3\,\text{mM}}{\text{min}}$	c

Source: (a) (Guyton and Hall 1996), (b) Calculated from model equations for consistency, (c) Definition, (d) Estimate.

Table 2: **Parameter Values**

A_S	Membrane area/cell	$7.67 \cdot 10^{-5}$ cm^2	e
C_m	Membrane capacitance	$1.0 \frac{\mu \mathrm{F}}{\mathrm{cm}^2}$	a
$[Na^+]_a$	$[Na^+]$ in arterial blood	140 mM	a
$[K^+]_a$	$[K^+]$ in arterial blood	5.4 mM	a
$[Cl^-]_a$	$[Cl^-]$ in arterial blood	110 mM	a
$[Pr]_a$	Protein concentration in arterial blood	1.45 mM	d
X_e	Number of protein molecules in interstitium	$3.94 \cdot 10^{-9} \mu$mole	e
z_e	Negative charges per protein molecule in interstitium	85.4	e
X_i	Number of protein molecules per cell	$3.83 \cdot 10^{-6}$ μmole	d
z_i	Negative charges per protein molecule in cell	1.44	e
z_v	Negative charges per protein molecule in capillary	24.4	e
g_{Cl}	Cl^- conductance	$2.81 \cdot 10^{-4}$ $\frac{\mathrm{mcoul}}{\mathrm{volt} \cdot \mathrm{min}}$	e
L_p^{ie}	Cell membrane water permeability	$1.21 \cdot 10^{12}$ $\frac{\mathrm{cm}^3}{\mathrm{Pa} \cdot \mathrm{min}}$	b
Q_a	Arterial blood flow	$3.6 \cdot 10^{-8}$ $\frac{\mathrm{cm}^3}{\mathrm{min}}$	e
$P_{\max}$	Maximum pump rate	$4.6 \cdot 10^{-8}$ $\frac{\mu\mathrm{mole}}{\mathrm{min}}$	c
K_{m,Na_i}	$[Na^+]_i$ half saturation for Pump	10 mM	c
K_{m,K_e}	$[K^+]_e$ half saturation for Pump	1.5 mM	c
g^b_{Na}	Background conductance of Na^+	$3.31 \cdot 10^{-5}$ $\frac{\mathrm{mcoul}}{\mathrm{volt} \cdot \mathrm{min}}$	e
g^b_{K}	Background conductance of K^+	$8.33 \cdot 10^{-4}$ $\frac{\mathrm{mcoul}}{\mathrm{volt} \cdot \mathrm{min}}$	e
$\overline{g_{\mathrm{Na}}}$	Maximum voltage-dependent conductance of Na^+	$3.69 \cdot 10^{-2}$ $\frac{\mathrm{mcoul}}{\mathrm{volt} \cdot \mathrm{min}}$	e
$\overline{g_{\mathrm{K}}}$	Maximum voltage-dependent conductance of K^+	$1.28 \cdot 10^{-2}$ $\frac{\mathrm{mcoul}}{\mathrm{volt} \cdot \mathrm{min}}$	e
τ_1	Extracellular volume elastic time constant	3.3 min	e
τ_2	Total volume elastic time constant	33.0 min	e
P^h	Coupling coefficient for ion transport	$6.0 \cdot 10^{-10}$ $\frac{\mathrm{cm}^3}{\mathrm{min}}$	e

Source: (a) (Guyton and Hall 1996), (b) (Baumgartner and Feher 1998),(Strieter et al. 1990), (c) (Luo and Rudy 1991), (d) Calculated from model equations for consistency, (e) Estimate.

References

Baumgartner, C. M. and J. J. Feher. 1998. In *Cell Physiology Source Book* (2 ed.). Osmosis and the regulation of cell volume. N. Sperelakis, editor. Academic Press, San Diego.Chapter 19 253–.

Beeler, G. W. and H. Reuter. 1977. Reconstruction of the action potential of ventricular myocardial fibers. *J. Physiol* 268:177–210.

Courtemanche, M., R. J. Ramirea, and S. Nattel. 1998. Ionic mechanism underlying human atrial action potential properties:insights from a mathematical model. *Am. J. Physiol.* 275: H301–H321.

DiFrancesco, D. and D. Noble. 1985. A model of cardiac electrical activity incorporating ionic pumps and concentration changes. *Phil. Trans. R. Soc. Lond. B* 307:353–387.

Fiolet, J. W., C. A. Schumacher, A. Baartscheer, and C. R. 1993. Osmotic changes and transsarcolemmal ion transport during total ischaemia of isolated rat ventricular myocytes. *Basic Res. Cardiol.* 88:396–410.

Fogelson, A. L. and N. T. Wang. 1996. Platelet dense-granule centralization and the persistence of ADP secretion. *Amer. J. Physiol.* 270:H1131–H1140.

Fogler, H. S.. 1986. *Elements of Chemical Reaction Engineering*. Englewood Cliffs, NJ: Prentice-Hall.

Fung, Y. C.. 1990. *Biomechanics: Motion, flow, stress, and growth*. New York: Springer-Verlag.

Guyton, A. C. and J. E. Hall. 1996. *Textbook of Medical Physiology*. Philadelphia, PA: Saunders.

Hansen, A. J.. 1978. The extracellular potassium concentration in brain cortex following ischemia in hypo- and hyperglycemic rats. *Acta Physiol. Scand. 102*(3):324–329.

Hill, J. L. and L. S. Gettes. 1980. Effect of acute coronary artery occlusion on local myocardial extracellular K^+ activity in swine. *Circulation 61*(4):768–777.

Hodgkin, A. L. and A. F. Huxley. 1952. A quantitative description of membrane current and its application to conduction and excitation in nerve. *J. Physiol.* 117:500–544.

Hrabetova, S., K. Chen, D. Masri, and C. Nicholson. 2002. Water compartmentalization and spread of ischemic injury in thick-slice ischemia model. *J Cereb Blood Flow Metab* 22: 80–88.

Hwang, T. C. and D. C. Gadsby. 1994. Chloride ion channels in mammmalian heart cells. In *Current topics in membranes*.Volume 42. Academic Press, San Diego. 317–346.

Jennings, R. B. and K. A. Reimer. 1991. The cell biology of acute myocardial ischemia. *Annu. Rev. Med.* 42:225–46.

Luo, C. H. and Y. Rudy. 1991. A model of the ventricular cardic action potential: depolarization, repolarization, and their interaction. *Circ. Res.* 68:1501–1526.

Noble, D., S. J. Noble, G. C. L. Bett, Y. E. Earm, W. K. Ho, and I. K. So. 1991. The role of sodium-calcium exchange during the cardiac action potential. *Annals of the New York Academy of Sciences* 639:334–353.

Patlak, C., D. Goldstein, and J. F. Hoffman. 1963. The flow of solute and solvent across a two-membrane system. *J. Theoret. Biol.* 5:426–442.

Strieter, J., J. L. Stephenson, L. G. Palmer, and A. M. Weinstein. 1990. Volume-activated chloride permeability can mediate cell volume regulation in a mathematical model of a tight epithelium. *J. Gen. Physiol.* 96:319–344.

Weiss, J. N. and P. Korge. 2001. The cytoplasm: No longer a well-mixed bag. *Circulation Research* 89:108–110.

Wilde, A., D. Escande, C. Schumacher, D. Thuringer, M. Mestre, J. Fiolet, and M. Janse. 1990. Potassium accumulation in the globally ischemic mammalian heart. *Circulation Research* 67:835–843.

Wilders, R., H. J. Jongsma, and A. C. G. van Ginneken. 1991. Pacemaker activity of the rabbit sinoatrial node: a comparison of mathematical models. *Biophys. J.* 60:1202–1216.

Yan, G. X., J. Chen, K. A. Yamada, A. G. Kleber, and P. G. Corr. 1996. Contribution of shrinkage of extracellular space to extracellular K^+ accumulation in myocardial ischemia of the rabbit. *J. Physiol.* 490:215–228.

Yan, G. X., K. A. Yamada, A. G. Kleber, J. McHowat, and P. B. Corr. 1993. Dissociation between cellular K^+ loss, reduction in repolarization time, and tissue ATP levels during myocardial hypoxia and ischemia. *Circ. Res.* 72:560–570.

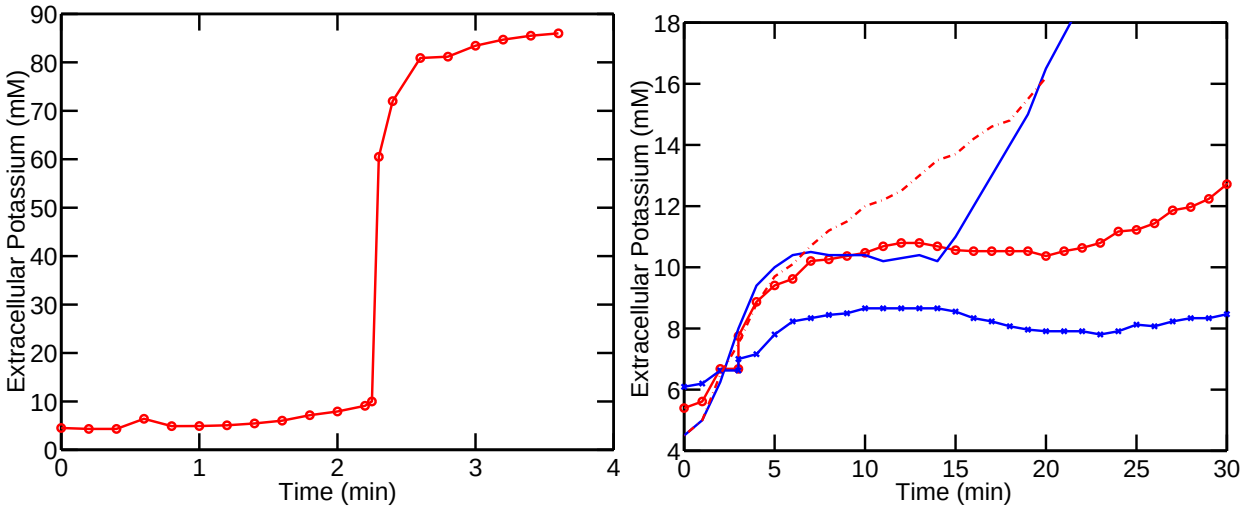

Figure 1: Extracellular Potassium $[K^+]_e$ vs Time. Left: Ischemia in brain tissue from (Hansen 1978). Right: Ischemia in cardiac tissue - center ischemic zone (O), border ischemic zone (X) in intact pig heart from (Hill and Gettes 1980), stimulated whole isolated rabbit heart (solid) from (Wilde et al. 1990), isolated blood-perfused rabbit papillary muscle (dashed) from (Yan et al. 1996).

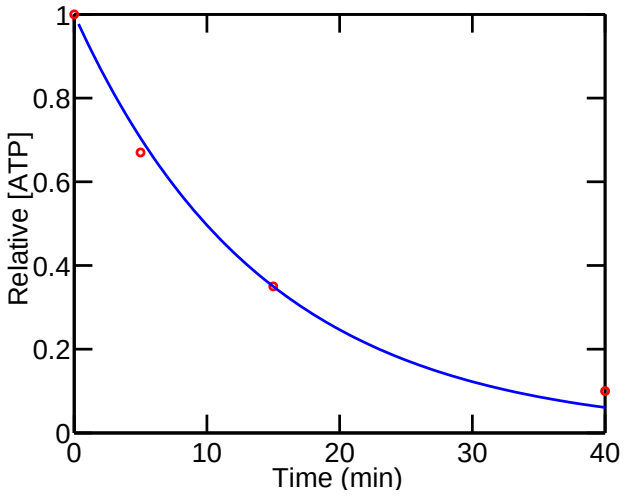

Figure 2: Relative tissue $[ATP]$ vs. time in ischemia and hypoxia fit to data from Jennings and Reimer (1991).

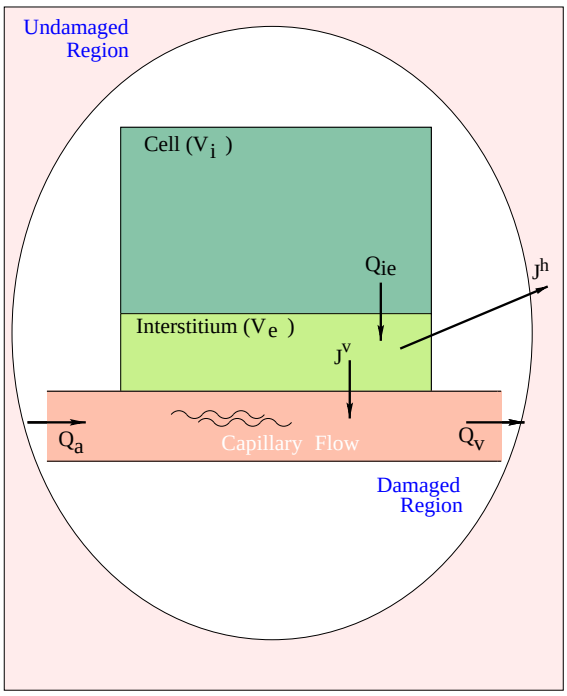

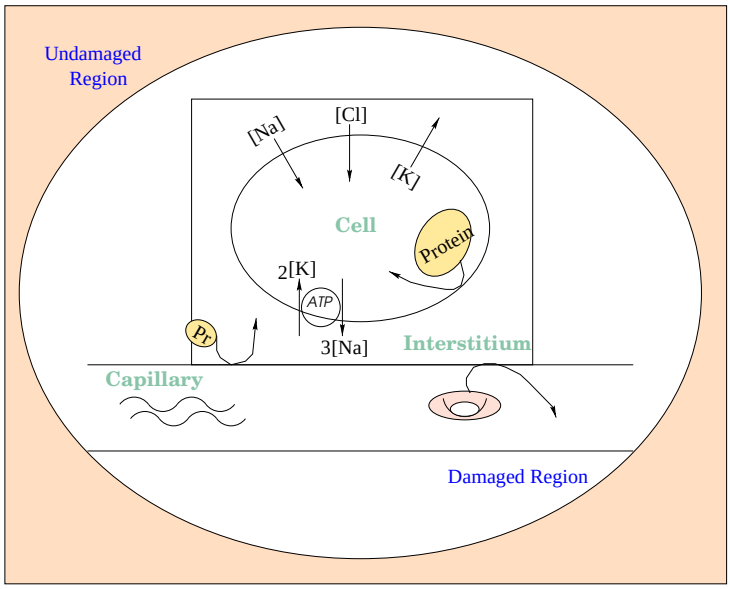

Figure 3: Top: Schematic diagram of the model. Bottom: The ionic components of the model.

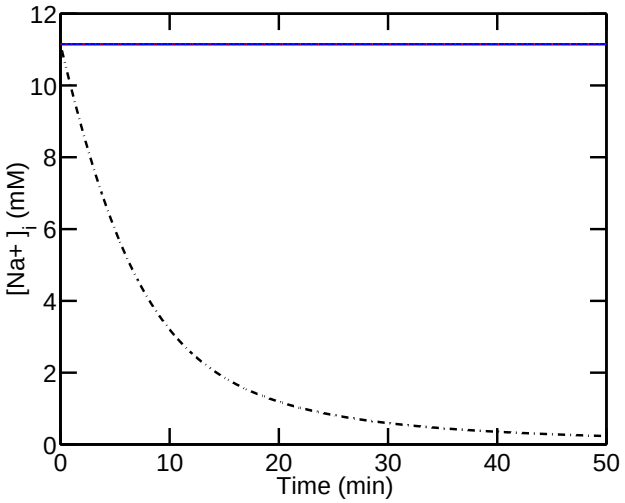

Figure 4: $[Na^+]_i$ vs time following a small perturbation from steady state for healthy tissue. Solid line shows steady state value. With nonzero $g^b_{\mathrm{Na}}$with set to value in Appendix, graph of $[Na^+]_e$ following perturbation is indistinguishable from the steady state curve. Dashed line shows $[Na^+]_e$ with $g^b_{\mathrm{Na}} = 0$.

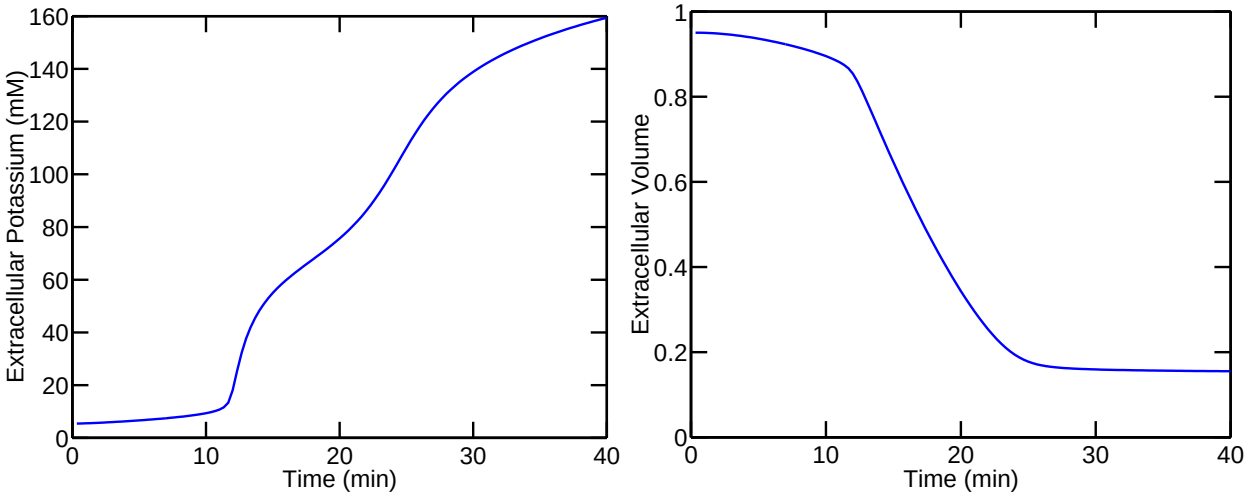

Figure 5: Simulation of ischemia with no coupling to healthy tissue. Left: Extracellular Potassium $[K^+]_e$. Right: Extracellular Volume V_e.

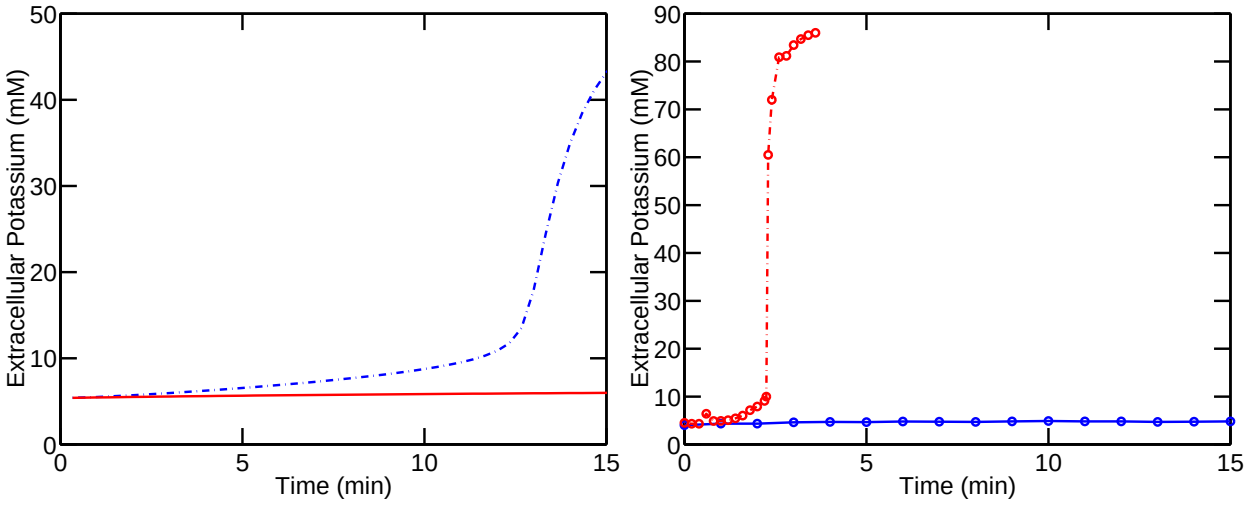

Figure 6: $[K^+]_e$ accumulation in ischemia (dashed) and hypoxia (solid). Left: Model results. Right: Experimental data from Hansen (1978) for neural ischemia (dashed) and Yan et al. (1993) for cardiac hypoxia (solid).

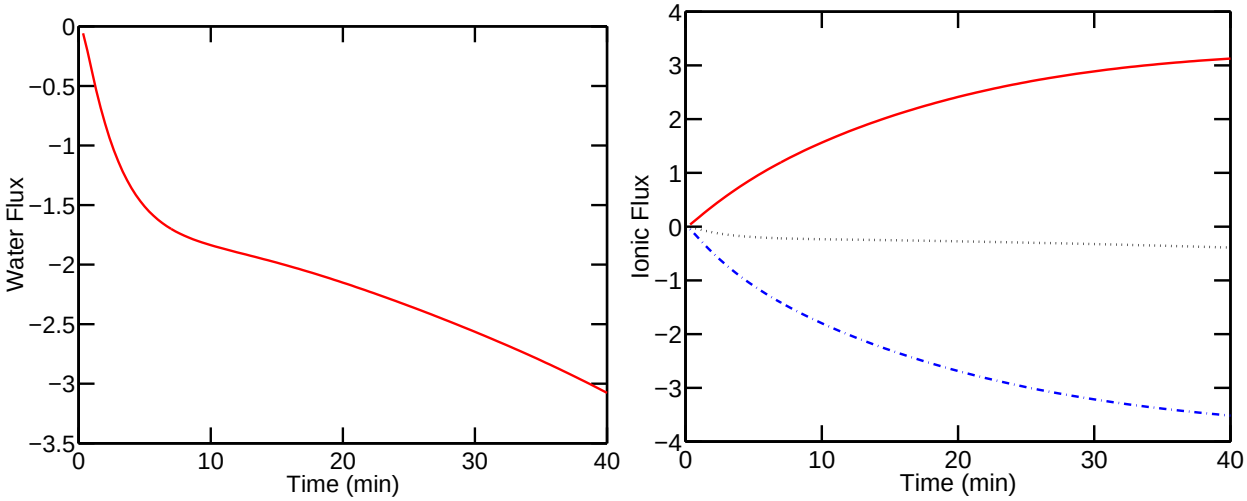

Figure 7: Water and ion fluxes across capillary wall during hypoxia. Left panel: $J^v_{\mathrm{H_2O}}$ in units of $10^{-11}\mathrm{cm}^3/\mathrm{min/cell}$. Water comes into the interstitium from the capillary at a rate almost the same as Q_{ie}. V_e is approximatively $9.5\cdot 10^{-9}\mathrm{cm}^3$. Right panel: J^v_{Na} (dash-dot), J^v_{K} (solid), and J^v_{Cl} (dot) in units of 10^{-11} mmol/min/cell. These have almost the same values as the corresponding ionic fluxes from the cell to the interstitium, so the extracellular ion concentrations change little. For reference, $V_e\cdot[Na^+]_e$, $V_e\cdot[K^+]_e$, $V_e\cdot[Cl^-]_e$ are approximately $1.3\cdot 10^{-9}$, $5.2\cdot 10^{-11}$, and $1.0\cdot 10^{-9}$ mmole, respectively. $J^v_{\mathrm{H_2O}}=0$, $J^v_{\mathrm{Na}}=0$, $J^v_{\mathrm{K}}=0$, and $J^v_{\mathrm{Cl}}=0$ during ischemia.

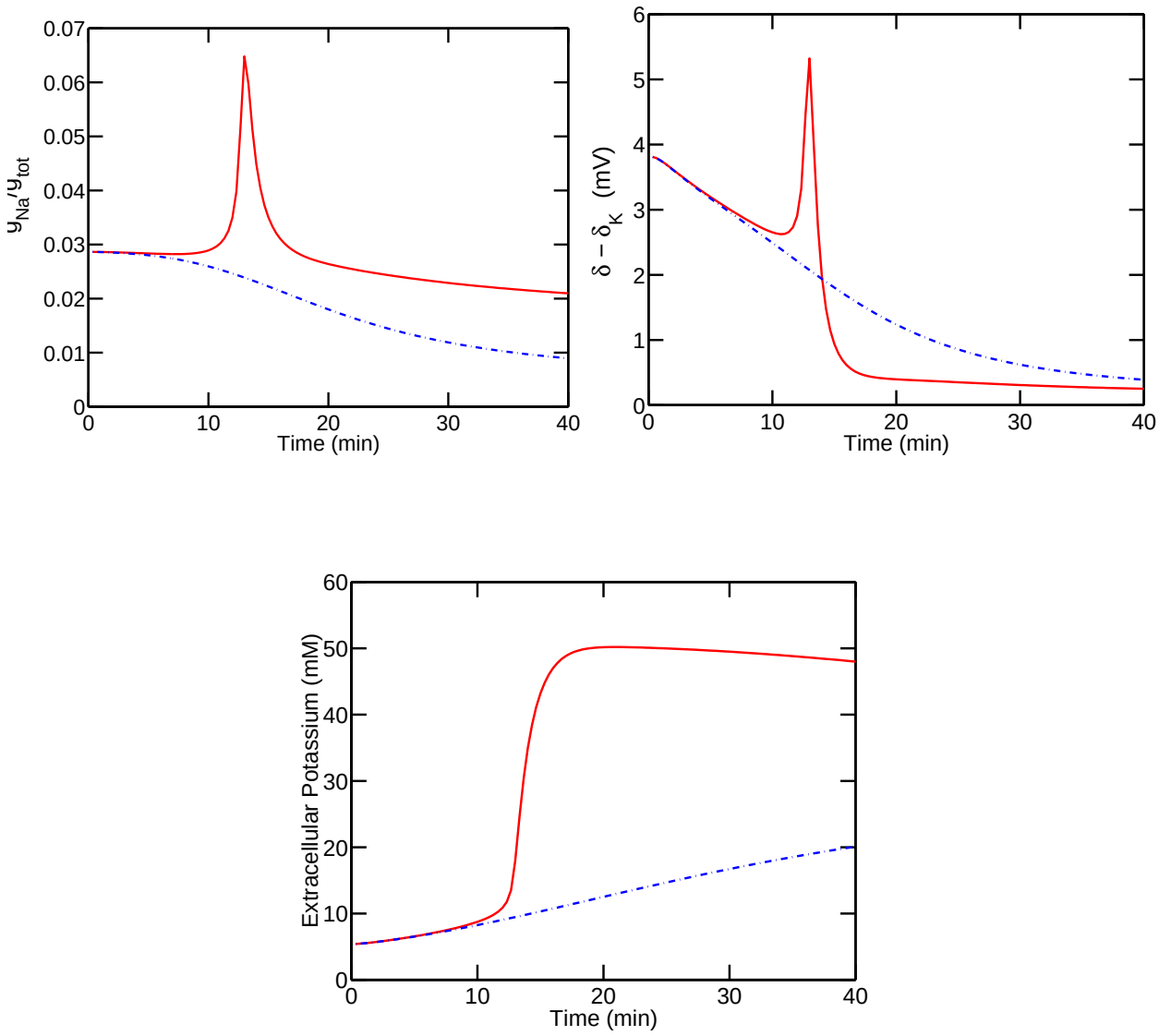

Figure 8: The effect of sodium conductance nonlinearity on $[K^+]_e$ rise in ischemia. Voltage-dependent g_{Na} gives solid curves. Constant g_{Na} gives dot-dashed curves. Top left: $g_{\mathrm{Na}}/g_{\mathrm{tot}}$. Top right: $\delta - \delta_K$. Bottom: $[K^+]_e$. The values of other parameters can be found in Appendix B.

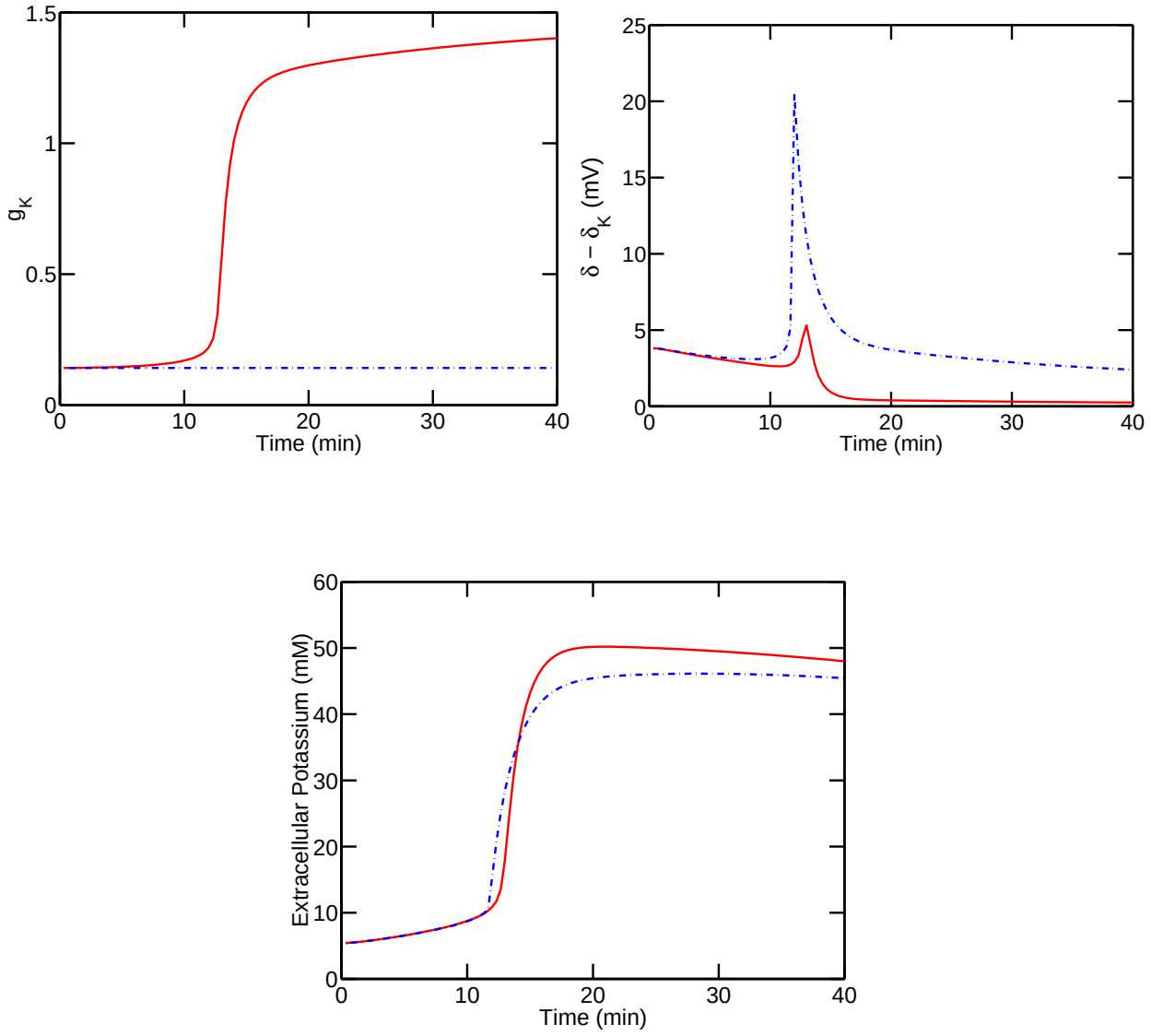

Figure 9: The effect of potassium conductance nonlinearity on $[K^+]_e$ rise in ischemia. Voltage-dependent g_{K} gives solid curves. Constant g_{K} gives dot-dashed curves. Top left: g_{K}. Top right: $\delta - \delta_K$. Bottom: $[K^+]_e$. The values of other parameters can be found in Appendix B.

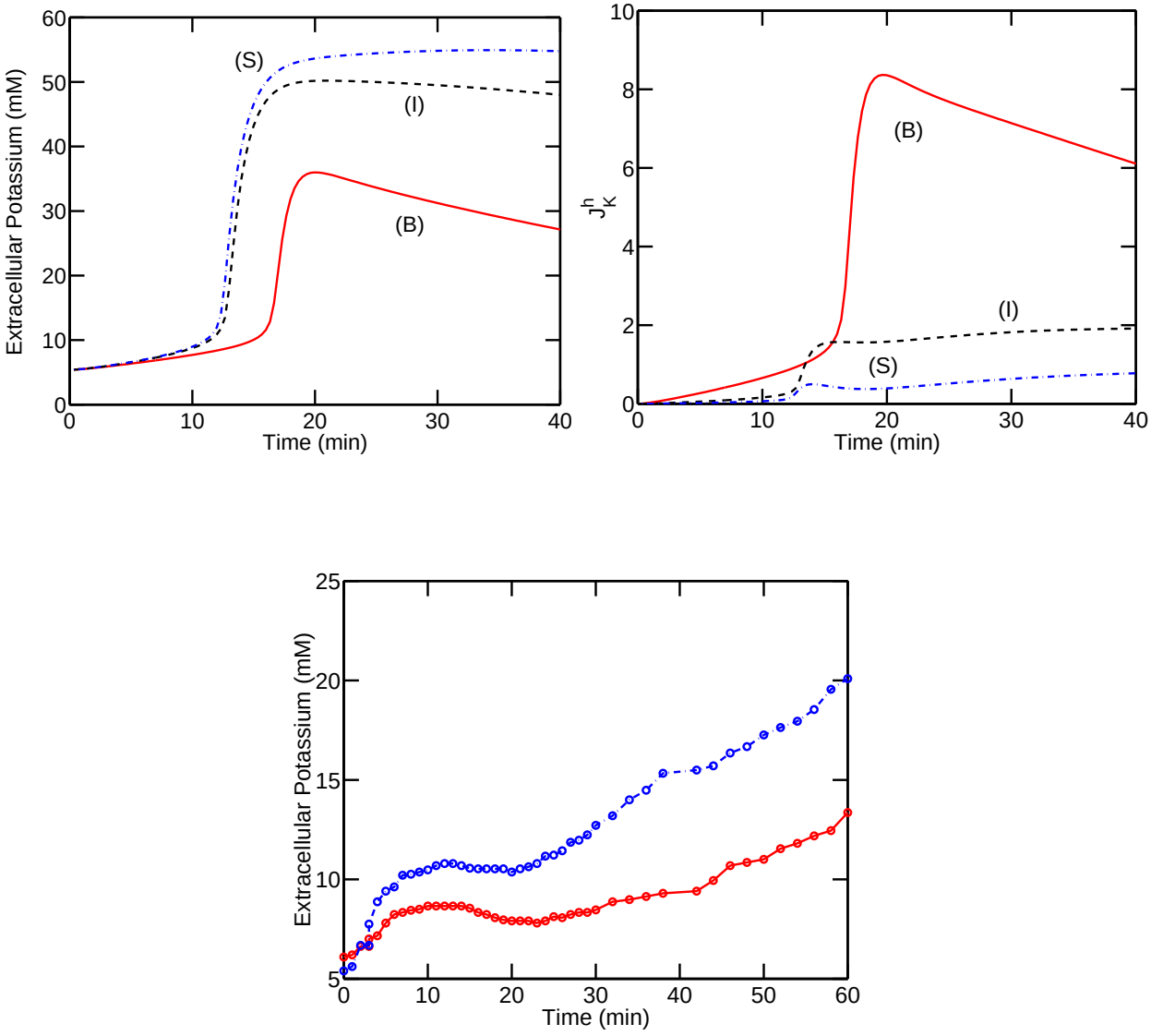

Figure 10: Extracellular potassium for different values of P^h. Larger values of P^h correspond to easier movement of ions between the ischemic tissue and the undamaged tissue. Top left: $[K^+]_e$. Top right: J_{K}^h. For three simulations $P^h = 3 \cdot 10^{-10}$ (S), $6 \cdot 10^{-10}$ (I), or $3 \cdot 10^{-9}$ (B) $\frac{\mathrm{cm}^3}{\mathrm{min}}$. Other parameter values can be found in Appendix B. Bottom: Experimental data for $[K^+]_e$ from different zones in cardiac ischemic tissue (Hill and Gettes 1980). Upper curve is for center of ischemic zone. Bottom curve is for border of ischemic zone.

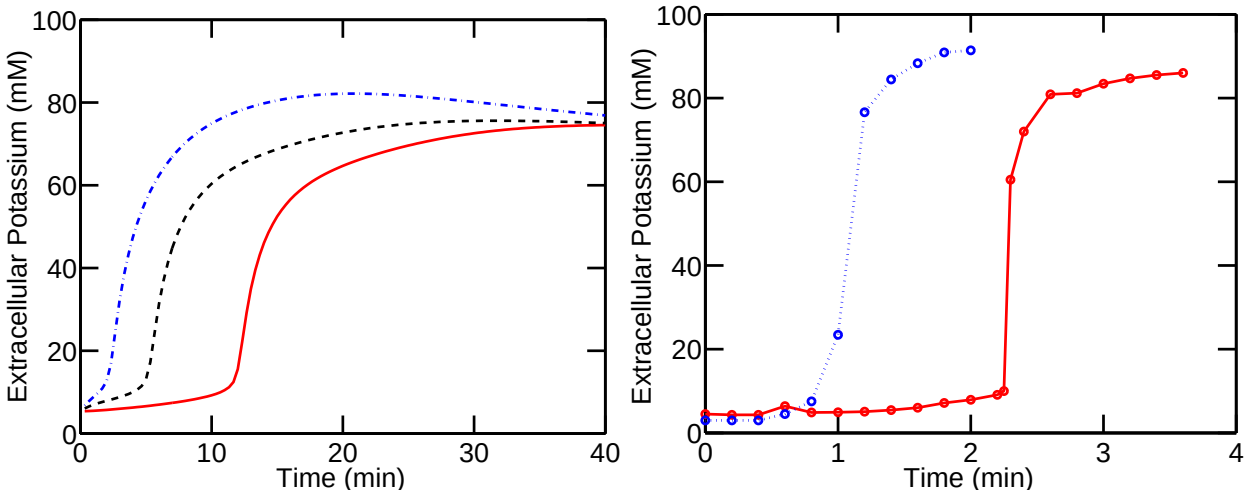

Figure 11: $[K^+]_e$ for different pump rates in ischemia. Left: Model calculation. Bottom curve is control with pump rate time curve given by function $a(t)$ fit to [ATP] data from (Jennings and Reimer 1991). Middle curve is with pump rate half of the control value at each time. Top curve is with pump rate equal to 0 for all times. Simulations use $g_{\mathrm{Cl}} = 0.061$ mS/cm^2, $P^h = 6.0 \cdot 10^{-11}$ cm^3/min, $\tau_1 = 18.5$min, $\tau_2 = 185$min, and other parameters as in Appendix B). Right: Data from Hansen (1978). Note different time scales. Bottom curve is with normoglycemic rats, top curve is with hypoglycemic rats.

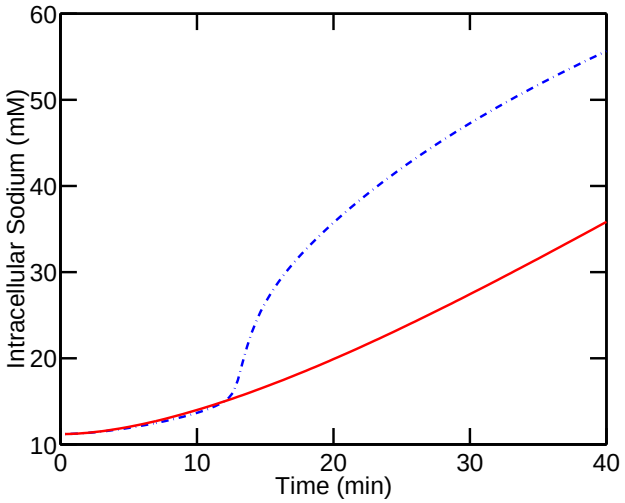

Figure 12: Calculated $[Na^+]_i$ accumulation during ischemia (dash-dot) and hypoxia (solid) using parameter values in Appendix B.

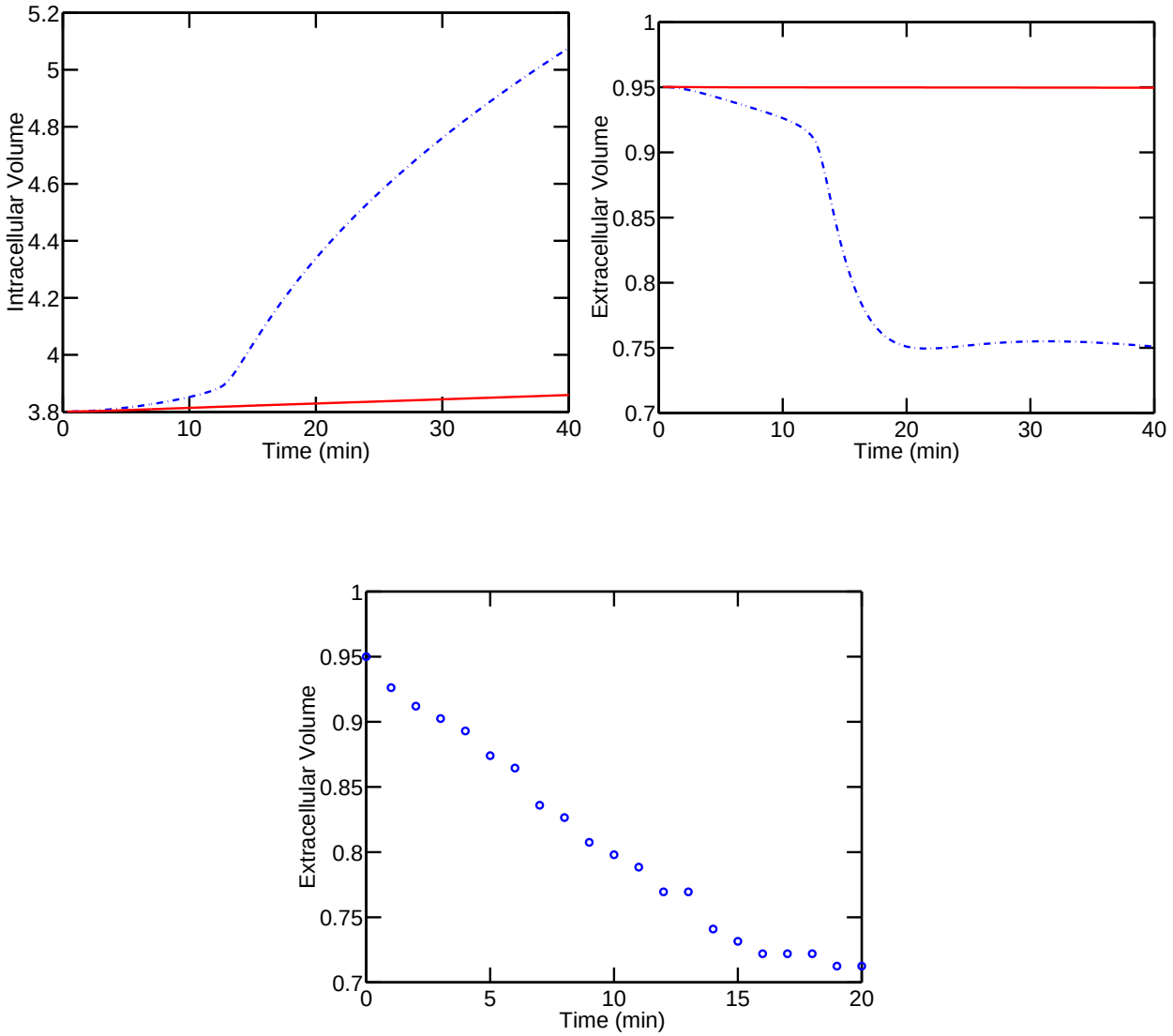

Figure 13: Comparison between ischemia and hypoxia. Left: V_i during hypoxia (solid) and ischemia (dashed). Right: V_e during hypoxia (solid) and ischemia (dashed). Volumes measured in units of 10^{-8}cm^3 per cell. The values of parameters can be found in Appendix B. Bottom: Experimental data for cardiac ischemia from Yan et al. (1996) rescaled so that normal volume is 0.95

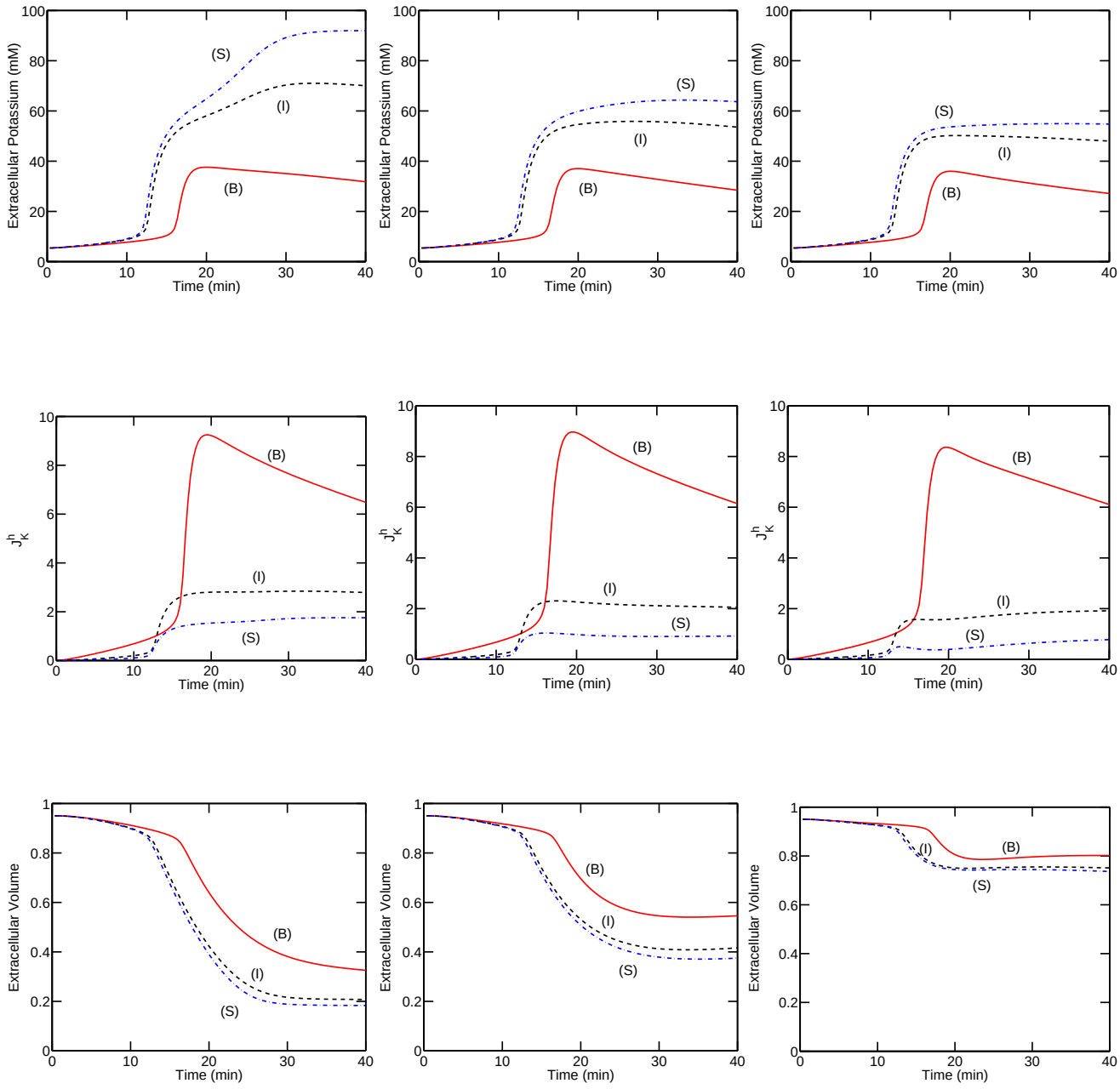

Figure 14: Comparison of $[K^+]_e$, $J^h_{\rm K}$, V_e during ischemia for different values of τ_1, τ_2 and different values of P^h. Left panels: $\tau_1 = 330$ min, $\tau_2 = 3300$ min. Middle panel: $\tau_1 = 18.5$ min, $\tau_2 = 185$ min. Right panel: $\tau_1 = 3.3$ min, $\tau_2 = 33$ min. For all experiments, $g_{\rm Cl} = 0.061\,{\rm mS/cm^2}$. For three experiments $P^h = 3 \cdot 10^{-10}$ (S), $6 \cdot 10^{-10}$ (I), or $3 \cdot 10^{-9}$ (B) ${\rm cm^3/min}$. Values of other parameters are in Appendix B.

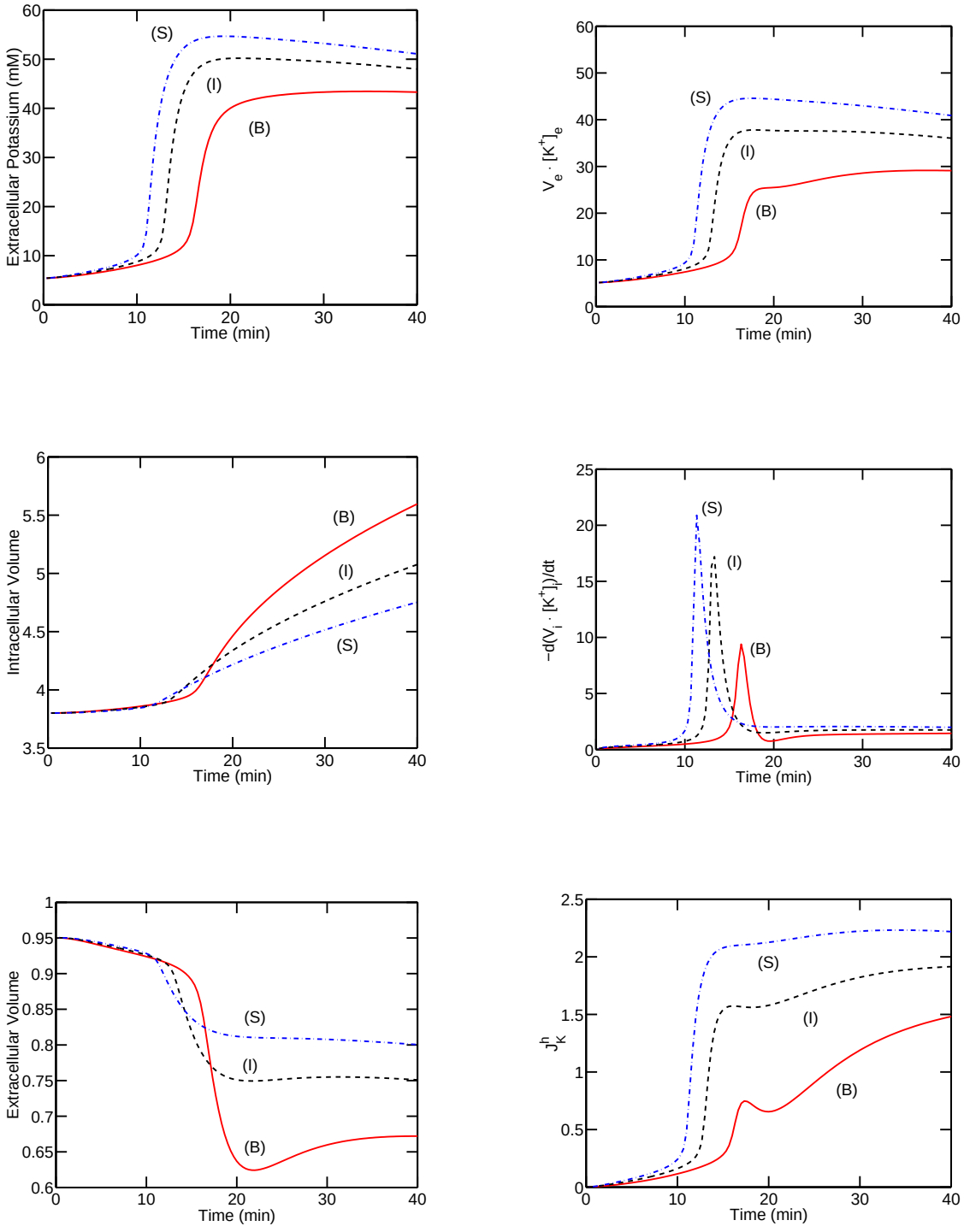

Figure 15: Influence of g_{Cl} on $[K^+]_e$ during ischemia: For three experiments g_{Cl} is 0.031 (S), 0.061 (I), 0.225 (B) mS/cm^2, respectively. Top left: $[K^+]_e$. Top right: $V_e \cdot [K^+]_e$ Middle left: V_i. Middle right: $-d(V_i \cdot [K^+]_i)/dt$. Bottom left: V_e. Bottom right: J^h_{K}. The values of other parameters can be found in Appendix B.

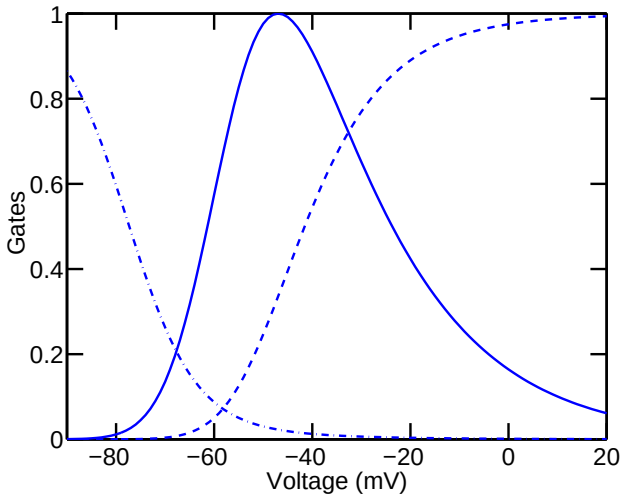

Figure 16: Steady-state behavior of sodium gates for Hodgkin-Huxley model: Solid: Relative $m_\infty^3(\delta) \cdot h_\infty(\delta)$. Dashed: $m_\infty^3(\delta)$. Dash-dot: $h_\infty(\delta)$.